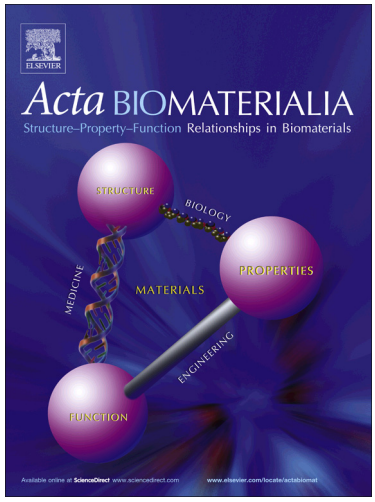

Full length article

Engineering Folate-Targeting Diselenide-containing Triblock Copolymer as a Redox-Responsive Shell-sheddable Micelle for Antitumor Therapy *In Vivo*

Farnaz Behroozi, Mohammad-Jafar Abdkhodaie, Hamid Sadeghi Abandansari, Leila Satarian, Mohammad Molazem, Khuloud T. Al-Jamal, Hossein Baharvand

PII: S1742-7061(18)30307-6
DOI: https://doi.org/10.1016/j.actbio.2018.05.031
Reference: ACTBIO 5484

To appear in: *Acta Biomaterialia*

Received Date: 7 January 2018
Revised Date: 8 May 2018
Accepted Date: 18 May 2018

Please cite this article as: Behroozi, F., Abdkhodaie, M-J., Sadeghi Abandansari, H., Satarian, L., Molazem, M., Al-Jamal, K.T., Baharvand, H., Engineering Folate-Targeting Diselenide-containing Triblock Copolymer as a Redox-Responsive Shell-sheddable Micelle for Antitumor Therapy *In Vivo*, *Acta Biomaterialia* (2018), doi: https://doi.org/10.1016/j.actbio.2018.05.031

Engineering Folate-Targeting Diselenide-containing Triblock Copolymer as a Redox-Responsive Shell-sheddable Micelle for Antitumor Therapy *In Vivo*

Farnaz Behroozi[1], Mohammad-Jafar Abdkhodaie[1,2*], Hamid Sadeghi Abandansari[3], Leila Satarian[4], Mohammad Molazem[5], Khuloud T. Al-Jamal[6], Hossein Baharvand[4,7*]

[1]Department of Chemical and Petroleum Engineering, Sharif University of Technology, Tehran, Iran

[2]Environmental Applied Science and Management, Ryerson University, Toronto, Canada

[3]Department of Cell Engineering, Cell Science Research Center, Royan Institute for Stem Cell Biology and Technology, ACECR, Tehran, Iran

[4]Department of Stem Cells and Developmental Biology, Cell Science Research Center, Royan Institute for Stem Cell Biology and Technology, ACECR, Tehran, Iran

[5]Department of Radiology and Surgery, Faculty of Veterinary Medicine, University of Tehran, Tehran, Iran

[6]Institute of Pharmaceutical Science, Faculty of Life Sciences & Medicine, King's College London, Franklin-Wilkins Building, London, UK

[7]Department of Developmental Biology, University of Science and Culture, Tehran, Iran

***Corresponding Author:**

abdmj@sharif.edu

and

Baharvand@Royaninstitute.org

Abstract

The oxidation-reduction (redox)–responsive micelle system is based on a diselenide-containing triblock copolymer, poly(ε-caprolactone)-bis(diselenide-methoxy poly(ethylene glycol)/poly(ethylene glycol)-folate) [PCL-(SeSe-mPEG/PEG-FA)$_2$]. This has helped in the development of tumor-targeted delivery for hydrophobic anticancer drugs. The diselenide bond, as a redox-sensitive linkage, was designed in such a manner that it is located at the hydrophilic–hydrophobic hinge to allow complete collapse of the micelle and thus efficient drug release in redox environments. The amphiphilic block copolymers self-assembled into micelles at concentrations higher than the critical micelle concentration (CMC) in an aqueous environment. Dynamic light scattering (DLS) and transmission electron microscopy (TEM) analyses showed that the micelles were spherical with an average diameter of 120 nm. The insoluble anticancer drug paclitaxel (PTX) was loaded into micelles, and its triggered release behavior under different redox conditions was verified. Folate-targeting micelles showed an enhanced uptake in 4T1 breast cancer cells and *in vitro* cytotoxicity by flow cytometry and (3-(4,5-dimethylthiazol-2-yl)-5-(3-carboxymethoxyphenyl)-2-(4-sulfophenyl)-2H-tetrazolium) (MTS) assay, respectively. Delayed tumor growth was confirmed in the subcutaneously implanted 4T1 breast cancer in mice after intraperitoneal injection. The proposed redox-responsive copolymer offers a new type of biomaterial for drug delivery into cancer cells *in vivo*.

Keywords: Redox-sensitive, Micelle, Diselenide, Breast cancer, Drug delivery

1. Introduction

Over the past decades, substantial research in cancer therapy has led to the development of polymeric drug delivery systems (DDSs) [1]. Polymeric micelles are considered to be one of the suitable candidates for DDSs. The micelles are formed by self-assembly of amphiphilic block copolymers into a spherical supramolecular core/shell nanostructure [2]. Poorly water-soluble anticancer agents can be encapsulated by physical entrapment into the hydrophobic core of the polymeric micelles [3]. The hydrophilic shell acts as a hydration barrier to provide colloidal stability and prolong the circulation time of nanoparticles by preventing rapid clearance from the bloodstream and uptake by the reticuloendothelial system (RES) [4,5]. Polyethylene glycol (PEG) is often used as a hydrophilic block owing to its acceptable biocompatibility, protein repulsion, lack of toxicity, and immunogenicity [6]. The biodegradable and biocompatible polyesters such as polycaprolactone (PCL), poly(D,L-lactic acid) (PLA), polyglycolic acid (PGA), and poly(lactide-co-glycolic acid) (PLGA) have been introduced as hydrophobic blocks [7-9]. In 2007, paclitaxel (PTX)-loaded poly(ethylene glycol)-b-poly(lactic acid) (PEG-b-PLA), termed Genexol-PM, was approved in Korea for the treatment of breast and mid-to-large–sized lung cancer cells [7]. Several other polymeric micelles have also entered clinical trials, such as NK105, NK911, NK012, and CriPec®-docetaxel [10]. Drug release in conventional micelles occurs by diffusion in addition to hydrolysis-induced biodegradation of the polyester micelles [11] and results in the nontargeted, insufficient, and uncontrolled release of the payloads. This inadequate accumulation of active drug within the cells leads to lack of therapeutic efficacy and drug resistance [12]. It is therefore necessary to increase the dosage of the administered drug to overcome this issue, and this often results in undesirable adverse effects.

Stimuli-responsive DDSs have attracted much attention recently owing to their potential for accurate and drug release in a controlled manner [13]. Among the mentioned stimuli such as pH [14], heat [15], oxidation–reduction (redox) potential [16], hypoxia [17], and enzymes [18], redox-responsive DDSs have demonstrated useful drug release behavior owing to the significant gradient in reducing potential among tumor and normal tissues. S-containing polymers, because of the reductive property of the sulfur (S) element, have proven to be ideal candidates for reductive-responsive disassembly for active anticancer drug release [19,20]. Shell-sheddable micelles, which contain a disulfide linkage between the hydrophilic and hydrophobic segments, have proven to exhibit a rapid intracellular drug release immediately after exposure to the reductive diseased region [21].

Inspired by the success of disulfide bonds, selenium (Se), an element listed in the family same as that of S in the periodic table of elements (chalcogens), has recently attracted considerable attention for not only their reduction responsiveness but also their sensitivity to low concentrations of oxidative agents [22]. In fact, Se-containing polymers have increased sensitivity and rapid responses to stimuli compared to disulfide analogs because of the weaker bond energy of the C-Se (244 kJ/mol) and Se-Se (172 kJ/mol) bonds than that of the C-S (272 kJ/mol) and S-S (240 kJ/mol) bonds [23,24]. Additionally, Se is involved in a wide range of biological functions such as antioxidant protection, thyroid function, gene transcription, cell growth, enhancement of the immune response, and anticancer activity [25–29]. Results indicate that the diselenide bond located between hydrophilic and hydrophobic segments is more preferred in case of diblock copolymers to ensure the complete collapse of a micelle when subjected to the redox stimuli, thus resulting in effective drug release [30]. It has also been shown that a diselenide bond is more sensitive than a disulfide bond, and the nanocarrier

containing diselenide has great potential for smart antitumor drug delivery [31]. Thus far, no studies have reported triblock copolymers with a diselenide linkage at the hydrophilic–hydrophobic hinge, as a micelle component.

In the following study, a dual reduction and oxidation (redox)–responsive triblock copolymer denoted as PEG-SeSe-PCL-SeSe-PEG [PCL-(SeSe-mPEG)$_2$], which contained a diselenide linkage between the hydrophobic (PCL) and hydrophilic (PEG) segments, was synthesized. The redox-sensitive triblock copolymer self-assembled into shell-sheddable micelles with a spherical core-shell structure in water. Higher specificity for cancer cells toward existing copolymers can be achieved by targeting the folate receptor, which is overexpressed on cancer cells [32,33] (Scheme 1). The disassembly of micelles and release of encapsulated anticancer drugs in the presence of oxidants or reductants were examined. In addition, careful evaluations of their *in vitro* and *in vivo* antitumor effects, cellular uptake, intracellular drug distribution, and systemic toxicity were performed. Our study concluded that the newly synthesized (PCL-(SeSe-mPEG)$_2$) copolymer offers a promising type of micellar carrier for controlled drug delivery for cancer therapy.

2. Materials and Methods

2.1. Materials

PCL diol (M_n=2000 Da); PEG methyl ether (mPEG, Mn=2000 Da); 3,3′-dithiodipropionic acid (DTPA); N,N′-dicyclohexylcarbodiimide (DCC); 4-(dimethylamino)pyridine (DMAP); triethylamine (TEA); chloroform; ammonium sulfate (AS); DL-Dithiothreitol (DTT); ethanol (EtOH); diethyl ether; and methanol were purchased from Merck (Germany). L-Glutathione (GSH); Se; trypsin-EDTA; dimethyl sulfoxide (DMSO); anhydrous tetrahydrofuran (THF);

sodium borohydride ($NaBH_4$); dimethylformamide (DMF); p-toluenesulfonyl chloride; hydrogen peroxide (H_2O_2); ammonia solution; 10-bromodecanoic acid 95%; dichloromethane (DCM); hexane; Hoechst 33342; Ca^{2+}-free and Mg^{2+}-free Dulbecco's phosphate-buffered saline (DPBS); phosphate-buffered saline (PBS); 4-(2-hydroxy-ethyl)-1-piperazineethane sulfonic acid (HEPES); deuterochloroform ($CDCl_3$); coumarin-6; 4′,6-diamidine-2′-phenylindole dihydrochloride (DAPI); Di-tert-butyldicarbonate (Boc_2O); folic acid (FA); magnesium sulfate ($MgSO_4$); dialysis tubing (MWCO=3500 Da); DCC; trifluoroacetic acid (TFA); and PTX were purchased from Sigma (St. Louis, MO, USA). RPMI-1640 medium and Alexa 488 dye were purchased from Invitrogen (Carlsbad, CA, USA). Fetal bovine serum (FBS); RPMI-1640 (without folic acid); penicillin; L-glutamine; and streptomycin were obtained from Gibco BRL (Rockville, MD, USA). A CellTiter 96 Aqueous One Solution Cell Proliferation Assay kit [containing 3-(4,5-dimethylthiazol-2-yl)-5-(3-carboxymethoxyphenyl)-2-(4-sulfophenyl)-2H-tetrazolium (MTS) and phenazine methosulfate (PMS)] was obtained from Promega (Madison, WI, USA). Ki-67 antibody (Abcam 15580) was purchased from Abcam (Cambridge, MA, USA). All other chemicals were of reagent grade and used as received.

2.2. Characterization

Fourier-transform infrared spectroscopy (FTIR) data were recorded on a PerkinElmer (RX I, USA) Fourier spectrometer at wavenumbers of the range 4000–400 cm^{-1} according to the KBr disk method. ^{1}H NMR spectra were acquired on a Bruker and Varian (400 mHz, Germany) NMR spectrometer. ^{77}Se-NMR measurements were acquired on a 500-MHz-Bruker-AV3-NMR spectrometer. The molecular weight (MW) was determined by gel permeation chromatography (GPC) (Agilent 110 HPLC, USA). Drug release profile was assessed using a high-performance

liquid chromatography (HPLC; Shimadzu, LC-10AT, China) system. Acetonitrile/water (50:50, v/v) was used as the mobile phase at 30°C with a flow rate of 1.0 mL/min. UV–Vis spectra were recorded using a Rayleigh UV-2601 (Beijing Rayleigh Analytical Instrument Co., Rayleigh UV-2601, China). The UV–Vis detector was set at 227 nm and linked to Breeze software for data analysis. Size distribution of micelles in aqueous solution was measured from three batches for each group in triplicates, using dynamic light scattering (DLS) carried out on a Malvern (Nano ZS90, UK) with a He–Ne laser (633 nm) and a scattering angle of 90°. Transmission electron microscopy (TEM) was performed using a JEM-2000CX, (JEOL Ltd., Japan) transmission electron microscope that had an accelerating voltage of 15 kV. The samples were prepared by pipetting a drop of the micelle solution (1 g/L) onto 230 carbon-coated mesh copper grids. The samples had to be air-dried before obtaining the measurements. The critical micelle concentration (CMC) of the PCL-(SeSe-mPEG)$_2$ copolymer in water was determined by using pyrene as the fluorescence probe in a Hitachi F-4500 fluorescence spectrophotometer (F-4500, Hitachi, Japan).

2.3. Synthesis and characterization of block copolymers

2.3.1. Synthesis of diselenide

Diselenide was prepared as previously described (Fig. 1A) [34]. Briefly, elemental Se (0.157 g, 1.99 mmol) and $NaBH_4$ (0.152 g, 3.98 mmol) were placed in a two-neck round-bottom flask and mixed under nitrogen gas flow. Then, 98% EtOH (0.7 mL) was added to the mixture until complete dissolution of Se and the formation of a white–gray solid. Subsequently, DMF (4 mL) was added to the solution, and this solution was then stirred until the formation of a red–brown color. Commercial 80% EtOH (0.45 mL) was continuously added to the mixture and vigorously

stirred until the end of gas production. Se powder (0.157 g, 1.99 mmol) was then added to the solution and stirred until the powder completely dissolved and a clear dark red solution was observed. Then, 10-bromodecanoic acid (1 g, 3.98 mmol) was added to the solution, thus resulting in a color change from red to yellow. After 24 h, the reaction was stopped by the addition of water (12 mL). The reaction mixture was extracted with diethyl ether (3×10 mL), and the extracted organic phase was washed with water (3×20 mL) and brine (15 mL). The organic phase was dried over $MgSO_4$ and filtered. The solvent was completely evaporated, and a yellow powder was obtained as the product with the following specifications: yield: 65%; ^{1}H NMR ($CDCl_3$, 400 MHz, δ): 1.22 (m, 20H, -CH_2), 1.50 (m, 4H, -***CH₂***CH_2Se-), 1.6 (m, 4H, -***CH₂***CH_2COOH), 2.2 (t, 4H, -***CH₂***Se-), and 2.8 (t, 4H, -***CH₂***COOH) (Figure 3A, B). ^{77}Se-NMR (1H-decoupled, THF-d8, 500 MHz): 303(s, Se_2). 2D ^{1}H,^{77}Se-HMBC (THF-d8, 500 MHz) (Figure 2A, B).

2.3.2. Synthesis of PCL-(SeSe-COOH)₂

HOOC-SeSe-PCL-SeSe-COOH (PCL-(SeSe-COOH)$_2$) was generated as follows. The PCL diol was allowed to react with excess diselenide by an esterification reaction (Fig. 1B). Briefly, a solution of DCC (1 mmol, 0.2 g) and DMAP (1 mmol, 0.12 g) were dissolved in THF (5 mL) and slowly dropped into a solution of PCL diol (0.1 mmol, 0.2 g) and diselenide (0.5 mmol, 0.25 g), dissolved in THF (5 mL). TEA (0.05 mL) was added to the reaction as a catalyst. The reaction was performed at room temperature (RT) under N_2 for 2 days. The polymer solution was filtered to remove DCU and concentrated by rotary evaporation. The concentrated filtrate was precipitated twice in diethyl ether. This precipitate was vacuum dried and had the following specifications: yield: 78%; ^{1}H NMR ($CDCl_3$, 400 MHz): δ 1.22 (m, 20H, -CH_2), 1.36 (m, 2H,

$COCH_2CH_2\boldsymbol{CH_2}CH_2CH_2O$), 1.65 (m, 4H, -$\boldsymbol{CH_2}CH_2O$), 2.31 (t, 2H, -$\boldsymbol{CH_2}COO$-), and 4.06 (t, 2H, -$\boldsymbol{CH_2}O$-) (Figure 3C).

2.3.3. Synthesis of the mPEG-amine

TEA (800 µl) was added to a solution of mPEG-OH (1 mmol, 2 g) in DCM (10 mL). p-Toluenesulfonyl chloride (1.99 mmol, 0.38 g) was then added in DCM (1 mL) dropwise to the vigorously stirred mixture. The reaction mixture was allowed to stir at RT overnight, after which this mixture was washed twice with a solution of NH_4Cl (500 mL). The organic phase was separated and dried over anhydrous $MgSO_4$. The solvent evaporated under pressure. The mPEG-OTs, as the solid product, were precipitated in diethyl ether and allowed to dry overnight in a vacuum oven. The dried product had the following specifications: yield: 83%; ^{1}H NMR ($CDCl_3$, 400 MHz): δ 2.37 (d, 4H, s, 6H, -CCH_3), 3.55 (m, 181H, PEG backbone, -O$\boldsymbol{CH_2}$-), 4.08 (t, 4H, -CH_2OTs), and 7.35-7.80 (d, 8H, aromatic ring) (Figure 3D).

mPEG-amine was prepared by dissolving 1.5 g of mPEG-OTs in an ammonia solution (80 mL), and this solution was stirred for 5 days at RT. The organic phase was separated and washed twice with DCM. The organic phase was dried over anhydrous $MgSO_4$, filtered, and evaporated under pressure. The concentrated filtrate was precipitated with cold diethyl ether, and the obtained mPEG-NH_2 was vacuum dried (white solid, 88%). The ninhydrin reaction was used to test for the presence of the amino group. The results indicated a yield of 78%; ^{1}H NMR ($CDCl_3$, 400 MHz, δ): 1.93 (broad peak, 4H, -NH_2), 3.42 (t, 4H, end -OCH_2- group), 3.67 (s, 181H, PEG backbone, -OCH_2-) (Figure 3E). PEG diamine (NH_2-PEG-NH_2) was also prepared by the same method.

2.3.4. Synthesis of PCL-(SeSe-mPEG)$_2$

PCL-(SeSe-mPEG)$_2$ was synthesized by an amide formation reaction between carboxyl groups of the synthesized PCL-(SeSe-COOH)$_2$ polymers and the amine group of mPEG-NH$_2$ (Fig. 1B). Briefly, PCL-(SeSe-COOH)$_2$ (0.04 mmol, 0.12 g) and mPEG-NH$_2$ (0.12 mmol, 0.24 g) polymers were dissolved in chloroform (15 mL). A solution of DCC (0.09 mmol, 0.018 g) and NHS (0.09 mmol, 0.01 g) dissolved in chloroform (5 mL) was added to the polymer solution. The coupling reaction between mPEG-NH$_2$ and PCL-(SeSe-COOH)$_2$ was carried out for 2 days at RT and under N_2 atmosphere. We filtered the copolymer solution to remove DCU, and the filtrate was slowly dropped into cold diethyl ether to precipitate the product as a white powder. The precipitate was vacuum dried at 30°C for 24 h. The dried product was dissolved in DMF and dialyzed against deionized water (DIW) with a dialysis membrane (MWCO=3.5 kDa) for 3 days. The dialyzed solution was lyophilized, and a white solid was obtained (Yield: 67.4%). ^{1}H NMR ($CDCl_3$, 400 MHz): δ 1.22 (m, 20H, -CH_2), 1.31 (m, 2H, $COCH_2CH_2$***CH_2***CH_2CH_2O), 1.57 (m, 4H, -***CH_2***CH_2O), 2.24 (t, 2H, -***CH_2***COO-), 3.58 (s, 181H, PEG backbone, -OCH_2-), and 3.98 (t, 2H, -***CH_2***O-)] (Figure 3F).

2.3.5. Synthesis of folate-conjugated block copolymer PCL-(SeSe-PEG-FA)$_2$

First, the PEG-diamine (NH$_2$-PEG-NH$_2$) was synthesized as described for mPEG-NH$_2$. One amine end group was protected with Boc_2O based on a previous report [35]. This copolymer had the following specifications: ^{1}H NMR ($CDCl_3$, 400 MHz, δ): 1.44 (S, 9H, -CH_3) and 3.64 (s, 181H, PEG backbone, -OCH_2-) (Figures 1C and S2A).

NH$_2$-PEG-NHBoC (0.87 mmol, 0.216 g) was allowed to react with FA (0.75 mmol, 0.330 g) in

the presence of dicyclohexyl carbodiimide (2 mmol, 0.41 g) in 30 mL of anhydrous DMSO/pyridine (3:1). The reaction proceeded at RT under N_2 atmosphere for 24 h. The resultant precipitate was filtered. The filtrate was then poured into a solution of cool diethyl ether to precipitate the product as a yellow powder. The precipitate was collected and dried under reduced pressure yielding FA-PEG-NHBoC. FA-PEG-NHBoC was unprotected by the reaction with TFA. Briefly, FA-PEG-NHBoC (0.045 mmol, 0.01 g) was dissolved in TFA (2 mL) and stirred for 3 h. TFA was completely removed under reduced pressure after which the residue was dissolved in DCM and precipitated in cold diethyl ether. The precipitate was collected and dried under reduced pressure to yield FA-PEG-NH_2 with the following specifications: ^{1}H NMR ($CDCl_3$, 400 MHz, δ): 3.57 (s, 181H, PEG backbone, -OCH_2-), 6.5, 6.7, 7.6, 7.7 (benzene ring), 6.9 (s, aromatic H of pteridine), and 8.7 (s, OH, 1H) (Figures 1C and S2B).

PCL-(SeSe-PEG-FA)$_2$ was synthesized by an amide bond formation reaction between the amine group of FA-NH-PEG-NH_2 and carboxyl groups of PCL-(SeSe-COOH)$_2$, as described for the PCL-(SeSe-mPEG)$_2$ preparation.

2.3.6. Synthesis of mPEG-PCL-mPEG

mPEG-PCL-mPEG copolymer was synthesized and used a control polymer. Initially, COOH-PCL-COOH was synthesized by a reaction of PCL diol with succinic anhydride. Briefly, PCL diol (1 g, 0.5 mmol) and succinic anhydride (0.4 g, 4 mmol) were added to dried dioxane (10 mL) and stirred until all reactants completely dissolved. DMAP (0.49 g, 4 mmol) and TEA (0.56 mL, 4 mmol) were added to the reaction mixture. The reaction was stirred for 24 h at RT under N_2 atmosphere. The solvent was evaporated in a rotary evaporator after which the concentrated cure product was precipitated in cold diethyl ether. This product had the following specifications:

yield: 89%.^{1}H NMR ($CDCl_3$, 400 MHz): δ 1.34 (m, 35H, -$COCH_2CH_2$***CH_2***CH_2CH_2O-), 1.56 (m, 70H, -$COCH_2$***CH_2***CH_2***CH_2***CH_2O-), 2.31 (t, 35H, - CO***CH_2***$CH_2CH_2CH_2CH_2O$-), 2.57 (m, 70H, -COO***CH_2CH_2***COOH), 4.06 (t, 35H, -$COCH_2CH_2CH_2CH_2$***CH_2***O-)] (Figure S2C).

Terminal carboxyl groups of HOOC-PCL-COOH were reacted with the amine group of mPEG-NH_2 *by* a coupling reaction as described for the PCL-(SeSe-mPEG)$_2$ preparation (Yield: 81.3%).

2.4. Preparation of micelles

The amphiphilic block copolymers (5 mg) were dissolved in DMF (2.5 mL) under vigorous stirring. The resultant solution was dialyzed against DIW by a dialysis membrane (MWCO=3.5 kDa) for 24 h, in which water replaced the DMF and the copolymers could self-assemble into nanomicelles. After 24 h, the dialyzed solution was filtered with a 0.45-μm filter and lyophilized.

2.5. Preparation of paclitaxel (PTX)-loaded micelles

PTX-loaded polymeric micelles were prepared according to the membrane dialysis method [36]. Briefly, PTX (5 mg) was added to the polymer solution (25 mg in 10-mL DMF) and stirred for 3 h at RT. The solution was then dialyzed against DIW for 24 h to remove the organic solvent and any unloaded PTX. The drug-loaded nanoparticle (NP) solution was filtered by a 0.45-μm filter to remove unloaded PTX**.** The PTX-loaded micelles were then freeze-dried.

Drug loading content (DLC) and drug loading efficiency (DLE) of these micelles were determined by HPLC according to previously reported procedures [37]. Briefly, drug-loaded micelles (5 mg) were dissolved in 1-mL DMF under vigorous vortexing. This solution was transferred to 5 mL of a mobile phase that consisted of DIW and acetonitrile (50:50, v/v). The samples were left overnight in a vacuum oven to evaporate water. Four hundred milliliters of

60% acetonitrile were added to the samples for HPLC analysis. A reverse-phase C_{18} column (250 mm x 4.6 mm; Agilent Technologies) was used with a flow rate of 1 mL/min for the mobile phase. The column effluent was detected at 227 nm using an UV-Vis detector. We calculated both DLC and DLE according to the following equations:

$$\mathrm{DLC(wt\%)} = \frac{\text{Weight of the loaded drugs in NP}}{\text{Weight of drug} - \text{loaded NPs}} \times 100$$

$$\mathrm{DLE(wt\%)} = \frac{\text{Weight of the loaded drugs in NP}}{\text{Weight of drugs in feed}} \times 100$$

2.6. *In vitro* L-Glutathione (GSH)- and hydrogen peroxide (H_2O_2)-triggered release of paclitaxel (PTX) from micelles

In vitro release profiles of PTX from micelles were investigated in three different buffers (all containing 1 M sodium salicylate) of PBS (0.01 mol/L, 1 M sodium salicylate, pH 7.4), 2 mM GSH, and 0.1 wt. % H_2O_2 by the diffusion technique using a dialysis bag [34]. Drug-loaded micelles (1.5 mL) were introduced into a dialysis membrane tubing (Spectra, MWCO=3.5 kDa) and incubated in 25 mL of buffer at 37°C. At predetermined time intervals, samples were drawn from each buffer and replaced with an equal volume of the same medium. The concentration of PTX in the solution was measured by HPLC as previously described.

2.7. Cell culture

Murine breast cancer cell line 4T1 (Cell Bank, Pasteur Institute of Iran) was cultured in RPMI-1640 with 5 g/L L-glutamine supplemented with 10% FBS, 100 U/mL of penicillin, and 100 mg/mL streptomycin. The cells were incubated at 37°C under humidified 5% CO_2 atmosphere. Passage-2 cells were used for all *in vitro* analyses. All cell studies were conducted in folic-acid free media except for competition studies were folic acid was added at 100 µg/ml.

2.8. Cytotoxicity and *in vitro* antitumor efficacy of micelles

MTS assay was used to evaluate the material cytotoxicity of the generated micelles in 4T1 cells. 4T1 cells were cultured in folate-free RPMI-1640 media 2 weeks before the cytotoxicity test was performed. A ready-for-use CellTiter 96® aqueous solution was used according to the manufacturer's protocol. 4T1 cells were seeded at a density of 5×10^3 cells/well and allowed to incubate for 24 h [38]. Then, the culture medium was replaced by 120 µL of the freshly prepared culture medium containing Taxol®, PCL-(SeSe-mPEG)$_2$, PCL-(SeSe-PEG-FA)$_2$, PTX-loaded PCL-(SeSe-mPEG)$_2$, or PTX-loaded PCL-(SeSe-PEG-FA)$_2$ micelles with equivalent concentrations that ranged from 0.01 to 1000.0 nM. After 24 h, the culture medium was removed and cells were rinsed with PBS. MTS stock solution (20 µL/well of MTS and 100 µL/well of cell media) was added to each well, cells were incubated for an additional 2 h, and absorbance was then measured at 490 nm by using a microplate reader (SpectraMax, M5, Sunnyvale, CA, USA) to calculate cell viabilities. The IC50 values were obtained by nonlinear regression curve-fit of the cell viability data with GraphPad Prism Software 7.0 (GraphPad Software, Inc., La Jolla, CA, USA).

2.9. Cellular uptake and intracellular drug release of coumarin-6–loaded micelles

The cellular uptake and intracellular drug release of loaded micelles were evaluated by loading coumarin-6 as a hydrophobic fluorescence marker for flow cytometry and confocal laser scanning microscopy (CLSM) analyses [39].

For flow cytometry analysis, 4T1 cells, maintained in folate-free RPMI-1640 media, were subcultured in a six-well plate (5×10^4 cells/well) for 24 h, followed by treatment with coumarin-6–loaded PCL-(SeSe-mPEG)$_2$ or coumarin-6–loaded PCL-(SeSe-PEG-FA)$_2$ at a final coumarin-6 concentration of 12.5 μg/mL. The free coumarin-6 was used as control at a concentration same as that of the coumarin-6 loaded in the micelle (12.5 μg/mL). Cells were subsequently rinsed thrice with PBS and harvested with trypsin, resuspended in PBS, and measured for fluorescence intensity (excitation: 450 nm, emission: 480 nm) on a BD FACSCalibur flow cytometer (Becton Dickinson, New Jersey, USA). The cellular uptake efficiency was calculated as follows:

$$\text{Uptake efficiency (\%)} = \frac{I_{sample}\text{-}I_{negative}}{I_{positive}\text{-}I_{negative}} \times 100\%$$

where I_{sample}, $I_{positive}$, and $I_{negative}$ represent the fluorescence intensities of the sample, positive (coumarin-6–loaded NPs in the cell lysis solution) control, and negative control (blank cell lysis solution), respectively. In this experiment, each particle suspension was added to five wells to study the effect of cellular uptake at 0.5- to 4-h time intervals.

For CLSM observation, 4T1 cells were seeded in 12-well glass-bottomed plates at a density of 1×10^5 cells/well in 1.5 mL of folate-free RPMI-1640 media and cultured for 24 h to reach an 80% confluence. The cells were then treated with coumarin-6–loaded PCL-(SeSe-mPEG)$_2$ or coumarin-6–loaded PCL-(SeSe-PEG-FA)$_2$, where the final concentration of coumarin-6 inside the micelle was maintained at 12.5 μg/mL. The free coumarin-6 was also used at a concentration of 12.5 μg/mL for 4 h [40]. Cells were rinsed thrice with PBS and fixed with 4%

paraformaldehyde for 20 min at RT. Finally, the nuclei were stained with Hoechst 33342 (10 μg/mL) in the culture medium for 10 min. The slides were mounted and observed by a confocal laser scanning microscope (Leica, TCS SP8, USA) equipped with excitation lasers (408 nm for the diode and 543 nm for He-Ne) and variable bandpass emission filters. All fluorescence images were captured using a microscope with the same setting parameters that included the intensity of the exciting light and exposure time for microscopy.

2.10. Animal study

2.10.1. 4T1 xenograft mice model

4T1 cells (5×10^6/100 μL of culture medium) were subcutaneously inoculated in the exponential phase of growth into the right flanks of 4-week-old (18–20 g) female BALB/c mice.

Mice were randomized into one of four experimental groups (n=6 per group) when tumors reached an average volume of 100 mm^3 [41]. Naked drug group was administered Taxol®, which was prepared by mixing a suspension of Taxol® in saline to create a 1.5-mg/mL PTX solution. All treated mice received intraperitoneal (i.p.) injections of Taxol®, PTX-loaded PCL-$(SeSe\text{-}mPEG)_2$, PTX-loaded PCL-$(SeSe\text{-}PEG\text{-}FA)_2$ at a PTX dosage of 15 mg/kg. The group injected with normal saline was assigned as a control. Treatments were administered every 4 days for six cycles as suggested in previous studies [42]. Tumor size was measured every 2 days using calipers for a 30-day period. Tumor volume was calculated as follows:

$$\text{Tumor volume } (mm^3) = 0.5 \times (L \times W^2)$$

where L and W are the length of major axis and width of minor axis, respectively. The Royan Animal Ethical Committee approved the animal study procedures.

2.10.2. Histology and immunohistofluorescence assay

Mice were euthanized on day 30. Tumor tissues were collected immediately, fixed in 4% paraformaldehyde for at least 24 h, and maintained in 30% sucrose/PBS until sectioning. The tumors were sliced with a thicknesses of 16 μm and stained with hematoxylin and eosin (H&E) for evaluation of any histopathological changes. The Ki-67 (1:100 dilution) antigen staining assay was conducted to evaluate antitumor efficacy on cell proliferation according to the manufacturer's protocol. In summary, the tissue sections were permeabilized with Triton X-100 and incubated with the antibody diluted in blocking buffer for 16 h. The cell nuclei were stained with DAPI (1.5 μg/mL of PBS solution) for 5 min. Paraffinized sections of organ tissues such as the lungs, heart, spleen, and kidneys were dewaxed in xylene, passed through a graded series of alcohol, rinsed in distilled water, and stained with H&E.

H&E- and Ki-67-stained sections were observed under a microscope (X51 Olympus; Olympus Corp. Tokyo, Japan). The extent of inflammatory changes that included macrophage and neutrophil localization, loss of blood, myofibrillar loss, cell atrophy, and fibrosis were assessed by a board-certified pathologist who had no knowledge of the study group assignments.

The apoptotic index was measured using the morphometric cell count (MCC) analysis that reports the apoptotic index as the total number of apoptotic cells versus the total number of cancer cells. Cell counts were performed by Image-Pro Plus 6.0 (Media Cybernetics, Inc., USA). The proliferation index was measured by the method same as that for apoptotic index, with the difference of reporting total numbers of proliferated cells (stained green cells in images) versus total numbers of cancer cells.

2.10.3. Myelosuppression and enzyme activity assay

Serum white blood cell (WBC) counts were assessed to study bone marrow suppression induced by the micelles. The blood samples were collected twice from each mouse (approximately 0.5 mL), once before starting the treatment and once on day 30 before they were sacrificed. WBCs were counted with the MEK-6318K Automated Hematology Analyzer (Nihon Kohden Corp., Japan).

Liver toxicity of the formulations was determined according to levels of the liver-specific enzymes serum glutamic oxaloacetic transaminase (SGOT) and serum glutamic pyruvic transaminase (SGPT). Serum SGOT and SGPT levels were determined using an autoanalyzer (Technicon RA1000 analyzer; Technicon Instruments, NY, USA) [43].

2.11 *In vivo* CT and ultrasound imaging of the tumor model

CT imaging was performed on a SOMATOM Spirit (Siemens, Berlin, Germany) scanner with the following parameters: beam collimation: 2 x 1 mm, beam pitch: 0.5 mm, gantry rotation time: 0.8 s, slice thickness: 1 mm, Kernel: (U 90) ultra-high resolution, and window: Osteo. All *in vivo* groups of 4T1 tumor-bearing mice were imaged. Evaluation of images was performed by loading the digital CT images in a standard display program (DICOM viewer) after which a uniform round region of interest in the CT image was selected for each sample. CT imaging was performed to measure the thoracic and abdominal cavities of each mouse at day 30.

Ultrasound images were acquired by using a GE Voluson 730 Pro (GE, Milan, Italy) ultrasound machine with a linear and phased array with a 7- to 12-MHz probe with a near-field setting. Data from dorsal recumbency under general anesthesia were obtained from female BALB/c 4T1 tumor-bearing mice at day 30.

2.12 Statistical analysis

Data were analyzed using GraphPad Prism version 6.01 (GraphPad Software, San Diego, CA, USA). Each experiment was repeated at least thrice unless otherwise noted. The mean value of the repetition was calculated and used for statistical analysis. For multiple groups, results were analyzed by one-way analysis of variance (ANOVA) followed by the Newman−Keuls test. A p-value of <0.05 was considered statistically significant (*p<0.05, **p<0.01, ***p<0.001).

3. Results and discussion

3.1 Synthesis and chemical characterization of the copolymers

Wei et al prepared a diselenide-centered biodegradable triblock copolymer $(mPEG–PCL–Se)_2$ that enabled the formation of self-assembled micelles [44]. In the previously reported study, the diselenide linkage was located in the core of the micelle, i.e., within the hydrophobic PCL chain and not at the PEG-PCL junction. The mechanism of drug release in the previous study is believed to occur through formation of pores of increasing sizes causing release of the anticancer drugs in a simulated tumor microenvironment. The use of shell-sheddable micelles may offer a more efficient stimuli-responsive drug release strategy, with drug release occuring as a result of micelle shell collapse [30]. In this study, we prepared a diselenide-bearing triblock copolymer in an attempt to develop a smart shell-sheddable micelle with sensitivity to redox environments. The proposed micelle has a hydrophilic outer shell that consists of mPEG, a hydrophobic core composed of PCL, and diselenide bonds located between the inner hydrophobic core and outer hydrophilic shell. This micelle can undergo shell shedding by breaking the diselenide bonds in a redox environment and subsequently release its payload. Figure 1 shows the synthesis of the copolymer. Initially, the bis(decanoic acid)-diselenide (diselenide) was synthesized by using 10-

bromodecanoic acid. Owing to solubility issues, we first introduced the diselenide group onto a long alkyl chain with carboxyl end groups, which possessed the desirable solubility in organic solvents [24]. The diselenide-containing amphiphilic block copolymer PCL-(SeSe-mPEG)$_2$ was then synthesized *by* a coupling reaction of PCL-diol with an excess amount of diselenide and finally terminated by PEG monomethyl ether and/or folate-conjugated PEG (Fig. 1).

^{1}H-NMR and FTIR spectra were obtained to confirm the chemical structures of the synthesized polymers. Figures 2 and 3 as well as Supplementary Figures S1 and S2 show the assigned characteristic peaks of the products. In the first step, diselenide was synthesized by a reaction between 10-bromodecanoic acid and Se powder in the presence of $NaBH_4$. ^{1}H-NMR confirmed the formation of bis(decanoic acid)-diselenide by shifting the peak at 3.40 ppm related to –***CH$_2$***-Br of 10-bromodecanoic acid to 2.86 ppm related to –***CH$_2$***-Se- of bis(decanoic acid)-diselenide (Fig. 3A,B). Further, ^{77}Se-NMR showed one clean peak at 303 ppm, related to Se-site (Figure 2A). In addition, the 2D ^{1}H,^{77}Se-HMBC indicated the presence of ^{77}Se attached to decanoic acid (Figure 2B). On the basis of the analysis conducted, it was confirmed that the diselenide compound was successfully synthesized. In the next step, PCL-(SeSe-COOH)$_2$ was synthesized by an esterification reaction of diselenide carboxyl groups and the hydroxyl end groups of the PCL-diol. The successful synthesis of PCL-(SeSe-COOH)$_2$ was confirmed by the characteristic peaks of methylene protons in PCL blocks at 1.40 ppm (-COCH$_2$CH$_2$***CH$_2$***CH$_2$CH$_2$O-), 1.54 ppm (-COCH$_2$***CH$_2$***CH$_2$***CH$_2$***CH$_2$O-), 2.25 ppm (-CO***CH$_2$***CH$_2$CH$_2$CH$_2$CH$_2$O-), and 3.97 ppm (-COCH$_2$CH$_2$CH$_2$CH$_2$***CH$_2$***O-) as shown in Figure 3C. The FTIR spectrum of PCL-(SeSe-COOH)$_2$ (Fig. S1) showed one band at 1734 cm^{-1}, which was related to -COO- band stretching vibrations in PCL. The broad band at 2500-3400 cm^{-1} was assigned to the terminal carboxyl groups of the diselenide segments. FTIR spectrum exhibited characteristic peaks of both diselenide and PCL

segments, which further confirmed the success of this synthesis (Fig. S1a). To add PEG as a hydrophilic block to the end of PCL-(SeSe-COOH)$_2$, the mPEG-NH$_2$ was synthesized in two steps by using PEG as an initiator. Initially, mPEG-OTs was synthesized by using mPEG-OH and p-toluene sulfonyl chloride. Next, mPEG-OTs was converted to mPEG-NH$_2$ by the addition of aqua ammonia by stirring. ^{1}H NMR spectra confirmed the successful preparation of mPEG-OTs and mPEG-NH$_2$ by showing the characteristic peaks of –CH$_2$-OTs and -CH$_2$-NH$_2$, respectively (Fig. 3D, E). Figure S1b shows the FTIR spectrum of mPEG-NH$_2$. Finally, PCL-(SeSe-mPEG)$_2$ with two separate diselenide groups in the hydrophobic–hydrophilic interface of the copolymer was prepared by the introduction of mPEG-NH$_2$ into the carboxyl end groups of (PCL-SeSe-COOH)$_2$ by an amide formation reaction. The appearance of a characteristic peak at 3.60 ppm was related to the methylene groups of PEG. The presence of characteristic peaks for PCL-(SeSe-COOH)$_2$ in the ^{1}H NMR spectrum of PCL-(SeSe-mPEG)$_2$ (Fig. 3F) showed the successful PEGylation of PCL-(SeSe-COOH)$_2$. FTIR spectrum analysis of the final PCL-(SeSe-mPEG)$_2$ also showed characteristic peaks of both PCL-(SeSe-COOH)$_2$ and mPEG-NH$_2$ segments, which demonstrated successful synthesis (Fig. S1c). The MW of PCL-(SeSe-mPEG)$_2$ was determined by GPC with experimental MW of 10,000 g/mol which is in close agreement with the theoretical value of 8500 g/mol (Fig. S5). In the GPC data, a clear secondary peak at a higher MW was observed, which could have been caused by the formation of an undesirable side product. For example, one possibility is that in the stage of PCL-(SeSe-COOH)$_2$ synthesis, a diselenide residue contributed to the formation of two or more PCL(Se-Se-mPEG)$_2$ adducts in the subsequent reaction. The amount, however, deemed to be negligible.

3.2. Preparation of micelles

The PCL-(SeSe-mPEG)$_2$ amphiphilic block copolymer formed core-shell–type micelles by self-assembly when exposed to an aqueous environment. The CMC of the amphiphilic PCL-(SeSe-mPEG)$_2$ copolymer was determined by fluorescence spectroscopy using pyrene as a hydrophobic probe molecule [45]. For fluorescence spectroscopy, the pyrene concentration in the final solutions was fixed at 6.0×10^{-7} mol/L, whereas the concentrations of the PCL-(SeSe-mPEG)$_2$ micelle varied from 5×10^{-4} to 5×10^{-1} mg/mL. The fluorescence intensity ratio of I_{372}/I_{384}, as a function of concentration was plotted to evaluate the CMC of the micelles prepared from copolymer PCL-(SeSe-mPEG)$_2$ (Fig. 4A(I)) [46]. As shown in Figure 4A(II), the CMC value of micelles was calculated to be 0.035 mg/mL. This CMC value guaranteed that the self-assembled micelle could retain its original morphology under highly diluted conditions *in vivo* before reaching the target site.

We evaluated the sizes of the micelles by dynamic light scattering (DLS). The results of DLS showed that PCL-(SeSe-mPEG)$_2$ copolymers formed micelles with an average size of 140 nm and polydispersity index (PDIs) of 0.2. Decorating micelles with folic acid did not change their size significantly as shown in the DLS and TEM data (Fig. S9). The mean zeta potential was approximately -0.1 mV. The PCL-(mPEG)$_2$ control group, without the diselenide linkage, was 110 nm and had a -0.05-mV zeta potential (Fig. 4B). The size and morphology of the micelles were further evaluated by TEM. As shown in Figure 4C, the micelles had a spherical morphology with an average diameter that ranged from 110 to 140 nm. We observed that the NPs were well separated from each other, which indicated that there was no aggregation between the micelles.

3.3. Redox-sensitivity of blank micelles

We designed this delivery system to be sensitive to both oxidative-rich and thiol-rich environments to fulfill the demand for clinical applications to release the drug in the intracellular region of cancerous cells. GSH, a thiol-containing chemical in the body, is present at a 100-1000 times greater concentration in the intracellular matrix compared to that in the extracellular environment [47]. The concentration of H_2O_2, as a reactive oxygen species (ROS) agent, in the intracellular region of cancer cells can increase to approximately 100 times higher levels than that in normal cells [48]. The size changes of the micelles during time were monitored by DLS in redox solutions to evaluate their redox-triggered disassembly. As shown in Figure 4B, the micelles maintained structural integrity in the redox-free buffer solution with no significant change in particle size for 4 h. However, we observed that diselenide-bearing micelles incubated in 2 mM GSH or 0.1% wt. H_2O_2 solutions created particles of various sizes. The obvious change in the size indicated that diselenide-bearing micelles dissembled into irregular particles owing to the cleavage of diselenide bonds by GSH and/or H_2O_2, which confirmed the sharp response of these micelles to the redox environment. The control micelles that lacked diselenide bonds maintained their structural integrity, with a diameter size of approximately 100 nm after incubation with 2 mM GSH for 4 h (Fig. 4B), which provided strong evidence that the redox sensitivity of micelles was attributed to the diselenide bonds. We also studied the cumulative release of carriers containing diselenide and folic acid to see whether conjugation to folic acid would affect the release pattern. For PCL-(SeSe-PEG-FA)$_2$, we observed a similar pattern to PCL-(SeSe-mPEG)$_2$ in 2 mM GSH and 0.1% H_2O_2 (not shown). This indicates that the inclusion of folic acid has no negative influence of the responsiveness of the diselenide-containing system.

3.4. Drug loading and release of micelles

We used the dialysis protocol to prepare the drug-loaded micelles. Hydrophobic anticancer PTX was readily integrated into the micellar core through hydrophobic interactions, and the excess PTX was removed by extensive dialysis. The theoretical DLC of the micelles was 21%. However, we calculated a DLE of 75%, as described earlier. Our DLC value is in agreement with those in the studies reported by others including Kim Yeon et al [49] and Wei Xiong et al [50], with reported values in the range of 16-20%. Our DLE of 80% is also in line with those in the studies by Jian Gong et al [51] and Zachar L. Tyreell et al [52].

To study the oxidative and reductive responsiveness of micelles, we investigated the release behavior of PTX-loaded micelles by using a dialysis tube containing micelles in three different buffer solutions (2 mM GSH, 0.1 wt. % H_2O_2, and PBS). The results showed that the PTX release rate from the micelles that contained diselenide significantly ($p<0.01$) increased in the redox environment compared to the control group (Fig. 5A). Approximately 75% of PTX was released from the diselenide-containing micelles with and without folic acid decoration, within the first 24 h, when exposed to 2 mM GSH buffer. Drug release reached nearly 100% after 75 h. The release pattern indicated that the carrier responded quite well to GSH, a thiol-rich molecule. Drug release from the same formulations was 35% and 45% within 24 h and 72 h, respectively, in the presence of 0.1% wt. H_2O_2. Drug release was less than 10% in the redox-free buffer solution within 75 h. The results indicated that the diselenide bond incorporated in our structure showed more sensitivity toward the reductive than oxidative environments. Furthermore, PTX release from diselenide-containing micelles was negligible under redox-free conditions. In

addition, the drug release behavior of the PCL-$(mPEG)_2$ micelles that lacked diselenide bonds was not affected by the redox environment (Fig. 5A). Cleavage of the diselenide bonds in the diselenide-containing micelles and shedding of the PEG shell along with aggregation of the PCL cores in the redox environment of a cancerous intracellular region resulted in a rapid PTX release compared to insensitive micelles and/or redox-free conditions. Furthermore, the stability of the micelles was monitored in 50% FBS (physiological condition). The size of PCL-$(SeSe\text{-}mPEG)_2$ particles incubated in 50% FBS for 20 days was measured by DLS. No significant change in size was observed (Fig. S6 A). Moreover, negligible release from PCL-$(SeSe\text{-}mPEG)_2$ + PTX was detected in 50% FBS, which increased to 44% release within 60 hours by addition of 0.1% H_2O_2 (Fig. S6 B). This result indicates that the carriers are stable under physiological conditions but release their payload when they are exposed to a redox environment.

This finding indicated that the diselenide bonds in micelles would not cleave in normal PBS buffer but were a function of the GSH or H_2O_2 present in the buffer.

3.5. Cytotoxicity and *in vitro* antitumor efficacy of micelles

MTS assay was used to evaluate biocompatibility and cytotoxicity of the proposed nano-sized carriers against 4T1 cells. The cells were incubated with varying amounts of the micelle concentration for 24 h. Figure 5B shows that the blank nanocarriers, which included PCL-$(mPEG)_2$, PCL-$(SeSe\text{-}mPEG)_2$, and PCL-$(SeSe\text{-}PEG\text{-}FA)_2$, had very low cytotoxicities with greater than 80% viability at all the concentrations (0.01-1000 nM). The results indicated that all the blank nanocarriers were biocompatible, nontoxic, and suitable for use as delivery systems of anticancer agents.

Cytotoxicity of diselenide- containing PTX-loaded micelles was dose dependent (Figure 5B and

Figure S7) ($p<0.001$) compared to the loaded nanocarrier that lacked diselenide. Data for the anticancer effect of the PTX-loaded PCL-(SeSe-PEG-FA)$_2$ and PTX-loaded PCL-(SeSe-mPEG)$_2$ on 4T1 cells showed that PTX-loaded PCL-(SeSe-PEG-FA)$_2$ had higher cytotoxicity even at PTX concentrations of 10 nM and lower compared to the PTX-loaded PCL-(mPEG)$_2$ ($p<0.001$). This implied that carriers that contained diselenide bonds were responsive to redox stimuli present in the region and released PTX *through* active targeting. On the other hand, PTX-loaded PCL-(mPEG)$_2$ micelles that lacked diselenide bonds did not have significant therapeutic effects in killing the cancerous cells.

Compared to passive diffusion of Taxol® through the cell membrane, the higher cytotoxicities of PTX-loaded PCL-(SeSe-PEG-FA)$_2$ and PTX-loaded PCL-(SeSe-mPEG)$_2$ have been attributed to the presence of diselenide and folate ($p<0.001$). Diselenide enhances targeted release of PTX in the cytoplasm of cancerous cells owing to its sensitivity to a thiol-rich and oxidative-rich environment. The improved toxicity of PTX-loaded PCL-(SeSe-PEG-FA)$_2$ compared to the nonfolate targeted version was attributed to the higher binding affinity of folate-decorated micelles to folate receptor (FR)–expressing 4T1 breast cancer cells [53].

We observed a greater cellular inhibition of PTX-loaded PCL-(SeSe-PEG-FA)$_2$ compared to PTX-loaded PCL-(SeSe-mPEG)$_2$ ($p<0.05$). At the 10 nM concentration, PTX-loaded PCL-(SeSe-mPEG)$_2$ reduced cell viability by approximately 50%, whereas PTX-loaded PCL-(SeSe-PEG-FA)$_2$ reduced cell viability by approximately 35% ($P<0.01$). We observed that PTX-loaded PCL-(SeSe-mPEG)$_2$ killed half of the cells at the 10-nM concentration, whereas PTX-loaded PCL-(SeSe-PEG-FA)$_2$ killed half of the cells at the 1 nM concentration. Compared to Taxol®, their IC50 values were 5.5-fold lower for PTX-loaded PCL-(SeSe-mPEG)$_2$ and 55-fold lower for PTX-loaded PCL-(SeSe-PEG-FA)$_2$. The results indicated that thiol- and oxidative-sensitive

PTX-loaded micelles demonstrated a higher antitumor effect in breast cancer cells compared to insensitive micelles and naked drug.

3.6. Cellular uptake and distribution of drug-loaded micelles in 4T1 cells

The therapeutic effects of drug-loaded micelles in cancer cells depend on internalization and sustained release of the carriers. Because PTX possesses no fluorescent characteristics to quantify the amount of intracellular uptake, we have used coumarin-6 as a hydrophobic fluorescent marker. We performed a time-course analysis (0.5 to 4 h) of couramin-6 uptake among different groups on 4T1 cells in the presence or absence of the micelles. Couramin-6 uptake was analyzed by FACS (Fig. 6A(I)). We treated passage-2 4T1 cells with coumarin-6-loaded PCL-(SeSe-mPEG)$_2$, coumarin-6-loaded PCL-(SeSe-PEG-FA)$_2$, and coumarin-6 (naked drug) at a drug concentration of 12.5 µg/mL. The control consisted of untreated 4T1 cells. There was a time-dependent increase in uptake from 0.5 to 4 h observed for all the micelle groups (data not shown). 4T1 cells showed the most uptake after 4 h. All other cell studies were conducted in folic acid–free media except for competition studies were folic acid was added at a concentration of 100 µg/ml.

The mean fluorescence intensity (MFI) of 4T1 cells treated with coumarin-6-loaded PCL-(SeSe-mPEG)$_2$ and PCL-(SeSe-PEG-FA)$_2$ was ~240 and ~719, respectively (Fig. 6A (II)). Because of the highly hydrophobic nature of coumarin-6, it readily partitioned into the lipid membranes and then diffused into the cells, which led to increased accumulation in these cells. We expected that owing to the increased expression of FR on 4T1 cells [54], the carriers that contained FA would have a higher internalization rate through FR. As shown in Figure 6A(I-II), cellular uptake of PCL-(SeSe-PEG-FA)$_2$ was at an average of 2-fold greater than PCL-(SeSe-mPEG)$_2$ micelles in

the 4T1cells. The uptake of PCL-(SeSe-PEG-FA)$_2$ was reduced when the culture media were supplemented with free folic acid at a concentration of 100 μM (Fig. S8). These findings altogether confirmed the active targeting capacity of the synthesized micelles, which supported the results of earlier studies [55].

Intracellular distribution of coumarin-6-loaded PCL-(SeSe-mPEG)$_2$ and PCL-(SeSe-PEG-FA)$_2$ micelles (12.5 μg/mL drug concentration, 4 h) was visualized in cells by CLSM (Figure 6B). The fluorescence intensity of coumarin-6 in cells was qualitatively observed by CLSM. The results agreed with the flow cytometry results shown earlier, which confirmed that coumarin-6-loaded PCL-(SeSe-PEG-FA)$_2$ had a stronger fluorescence intensity in the 4T1 cells than coumarin-6-loaded PCL-(SeSe-mPEG)$_2$. In the FA micelle–treated groups, coumarin-6 (green) was found densely dispersed around the blue nuclei (stained by DAPI), which implied that a higher number of fluorescently loaded micelles internalized into the 4T1 cells *through* the FR compared to the groups that lacked FA.

The intracellular uptake and distribution of coumarin-6 of PCL-(SeSe-PEG-FA)$_2$ was higher than that of PCL-(SeSe-mPEG)$_2$ in 4T1 cells that overexpressed FR. These data demonstrated that the conjugated FA further enhanced the tumor cell targeting effect and cellular uptake of coumarin-6-loaded PCL-(SeSe-PEG-FA)$_2$ *through* FR-mediated endocytosis, which promoted the entry of coumarin-6-loaded PCL-(SeSe-PEG-FA)$_2$ into FR-overexpressed 4T1 cells. In addition, based on the flow cytometry analysis (Fig. 6A(I)), we noted that the fluorescence intensity level of coumarin-6-loaded PCL-(SeSe-PEG-FA)$_2$ was much brighter than that of coumarin-6-loaded PCL-(SeSe-mPEG)$_2$. This confirmed that the FA-containing micelles were more efficiently internalized.

The cytotoxicity assays performed against 4T1 tumor cells with PTX-loaded micelles showed that PTX-loaded PCL-(SeSe-PEG-FA)$_2$ had a higher killing effect than PTX-loaded PCL-(SeSe-mPEG)$_2$ in these cells. This was in agreement with the cell uptake results, which showed that because of the presence of FA, we had higher internalization of FA-conjugated micelles and a higher accumulation of PTX. This led to enhanced drug cytotoxicity against the 4T1 cells.

3.7. *In vivo* antitumor effect

The tumor targeting capability of a DDS is critical for improving its antitumor activity. We have evaluated the *in vivo* antitumor effect and targeting of the micelles in a xenograft 4T1 murine breast cancer model. Based on results obtained from the *in vitro* studies, the smart micelles demonstrated satisfactory results; hence, we proceeded further for *in vivo* experiments. Figure 7A shows the progress of tumor volume growth during 30 days with different formulations of PTX-loaded smart micelles, free drug (Taxol®), and saline (control). Compared with the control and Taxol® groups, the smart micelle-treated groups exhibited a slower growth rate in tumor volume. The two micelle groups had a better inhibitory effect against tumor growth than the other groups, even when drug injection was stopped ($p<0.001$).

Remarkably, the average tumor volumes of the PTX-loaded PCL-(SeSe-PEG-FA)$_2$ and PTX-loaded PCL-(SeSe-mPEG)$_2$ treated groups were significantly smaller than the volumes of the saline and Taxol®-treated groups on day 30. This could be attributed to an enhanced permeation and retention (EPR) effect of nano-sized micelle delivery systems [56, 57]. In addition, the passively targeted PTX-loaded PCL-(SeSe-PEG-FA)$_2$ micelle that accumulated in the solid tumor region might be taken up more readily by 4T1 cells *through* a receptor-mediated endocytosis process. A combined effect of the passive targeting and enhanced cellular uptake

would be the main reason for the slow growth rate in tumors treated with PTX-loaded PCL-(SeSe-PEG-FA)$_2$. No statistically significant difference in antitumor effects between PTX micelles with or without FA was observed in the *in vivo* therapy study. One may propose that this may be due to the immature release of the drug from the micelles following i.p. injection. This hypothesis although cannot be disproven without conducting a pharmacokinetic/biodistribution experiment tracking both the free drug and the micelle to determine whether the micelles deliver the drug to the tumor and how much of the injected dose accumulates in the tumor, one can see the difference in histological analysis between the two groups, i.e., ~80% tumor tissue necrosis in the PTX-loaded PCL-(SeSe-PEG-FA)$_2$+PTX group and ~64% for the PTX-loaded PCL-(SeSe-mPEG)$_2$ group. A similar behavior in attaining significant differences in tumor sizes while changes at cellular levels could still occur has been observed in other studies using other types of tumors/carriers [58]. It is possible that the fast-growing nature of this tumor type (doubling time: 14.2 hours) [59] surpasses the changes in biochemical/histological event among the treatment groups. There is less concern about the EPR effect of 4T1 tumors, as they have been proven leaky when testing other types of nanocarriers [60]. Future studies will attempt the intravenous injection to ensure that the micelles encounter less biological barriers before reaching the tumor *by* the EPR effect, e.g., interaction with high–protein content i.p. fluids and drainage into lymphatic capillaries.

Figure 7B shows the changes in body weight of the different mice groups, as a safety indication, during the therapeutic experiment. Each group was compared to itself (for example, the weight of the Taxol® group was compared to that of the Taxol® group at different time points) in terms of increase or decrease in weight. No significant reduction in body weight in the mice that received the PTX-loaded PCL-(SeSe-mPEG)$_2$ and PTX-loaded PCL-(SeSe-PEG-FA)$_2$ micelles

were observed, which indicated reasonable safety levels and minimum side effects of these formulations. On the other hand, mice that received free Taxol® had evidence of weight loss during the treatment, and this might indicate adverse treatment effects and systemic toxicity.

Significant tumor inhibition in the groups treated with PTX-loaded PCL-(SeSe-mPEG)$_2$ and PTX-loaded PCL-(SeSe-PEG-FA)$_2$ was observed. This finding supported the observed results from the *in vitro* tests. Figure 7A shows that no significant difference existed in tumor growth rate between the PTX-loaded PCL-(SeSe-PEG-FA)$_2$ and PTX-loaded PCL-(SeSe-mPEG)$_2$ groups. H&E staining of tumors treated with folate micelles showed a high degree of necrosis and areas empty of cells (Fig. 9 A, B). This demonstrated that the antitumor effect of the active targeted system PTX-loaded PCL-(SeSe-PEG-FA)$_2$ was stronger than those of PTX-loaded PCL-(SeSe-mPEG)$_2$ and Taxol®, which could be due to the combined effect of passive targeting *through* EPR- and FR-mediated enhanced intracellular delivery. Tumor growth was inhibited in both groups of smart micelles compared to the Taxol®-treated group which indicated that redox-sensitive micelles led to a greater accumulation of Taxol® in the tumor.

In this study, the formulation was administrated *through* the i.p. route as a proof of concept study. Future studies will explore the i.v. route as a more clinically relevant route. Preliminary unpublished work demonstrated that these formulations did not result in mice death at the doses reported in this study. Additional work investigating the biocompatibility after i.v. injection is, however, still required.

3.8. Histological investigation of organ damage

H&E staining showed the presence of drug-related toxicities to the major organs in the PTX-loaded PCL-(SeSe-PEG-FA)$_2$– and PTX-loaded PCL-(SeSe-mPEG)$_2$–treated groups compared

to the saline and Taxol® groups on day 30. Figure 8 shows that the control group had liver and spleen damage. The Taxol® group had damage to the liver, heart, spleen, and lungs. The control group had evidence of metastatic seeding of breast cancer cells in the liver, spleen histiocytosis, and depletion of lymph nodules. The Taxol® group had evidence of the following damages to the heart (Zenker's necrosis and atrophy of myocardial cells), kidneys (mild hyperemia), spleen (histiocytosis), lungs (thickening of the alveolar walls and inflammatory cell infiltration), and liver (metastatic seeding of breast cancer cells). By contrast, the PTX-loaded PCL-(SeSe-PEG-FA)$_2$– and PTX-loaded PCL-(SeSe-mPEG)$_2$–treated groups had significantly less damage to the heart, lungs, liver, and spleen. These findings demonstrated the safety and therapeutic effect of the prepared micelles at the treated dose.

3.9. Tumor histological and immunofluorescence analysis

Histological and immunofluorescence analyses were performed on tumor tissues to further investigate the suppression efficiencies of PTX-loaded PCL-(SeSe-mPEG)$_2$ and PTX-loaded PCL-(SeSe-PEG-FA)$_2$. According to Figure 9A, H&E staining of normal 4T1 cells showed the presence of rhombic or polygonal cells and large purple nuclei with spherical or spindle shapes. The apoptotic cells shrank and turned into a round shape with condensed nuclei and became darker. Necrotic cell cytoplasm became a pink amorphous material, and the nucleus disappeared [61].

H&E results confirmed the *in vivo* antitumor effects of the micelle groups. Some degrees of apoptosis and necrosis were observed in the PTX-loaded PCL-(SeSe-PEG-FA)$_2$ and PTX-loaded PCL-(SeSe-mPEG)$_2$ tumor-treated groups. The folate-decorated micelles had larger necrotic areas in the tumor tissue, which indicated that these groups of micelles had better antitumor

effects compared to the control and Taxol® groups. By contrast, Figure 9A shows the H&E-stained tumor tissues from the control and Taxol® groups. In these two groups, the tumor cells had large nuclei, a spherical shape, and high mitotic figures, and these indicated rapid tumor growth.

The necrosis values for tumor tissues were less than 20% ($p<0.001$) for the Taxol® and saline groups (Fig. 9B(I)). By contrast, there was 80% tumor tissue necrosis in the PTX-loaded PCL-(SeSe-PEG-FA)$_2$+PTX group and 64% for the PTX-loaded PCL-(SeSe-mPEG)$_2$ group ($p<0.001$). These findings were in agreement with results of the previously reported antitumor effect. The micelles showed a better therapeutic effect of killing breast cancer cells and suppression of tumor growth than the naked drug.

Ki-67 staining assay was performed to further investigate tumor suppression *by* this proliferation assay for the different treatment groups. As shown in Figure 9B(II), 86% of the control group expressed Ki-67 and 73% of the Taxol® group expressed Ki-67 ($p<0.001$), which indicated active cell proliferation. PTX-loaded PCL-(SeSe-PEG-FA)$_2$ and PTX-loaded PCL-(SeSe-mPEG)$_2$ groups showed less than 5% and 10% Ki-67 positive cells ($p<0.05$), respectively, thus suggesting reduced active cell proliferation and increased inhibition of tumor growth in the micelle groups compared to the control and Taxol®-treated groups. These results presented substantial evidence for the high antitumor activity of the smart micelle groups, particularly the PTX-loaded PCL-(SeSe-PEG-FA)$_2$ group.

3.10. Myelosuppression assay

Bone marrow suppression is considered a serious toxicity of PTX [62]. Myelosuppression by micelles and PTX was evaluated by monitoring WBC counts before and after administration. As

shown in Figure S3A, Taxol® induced a significant decrease in WBC levels from 10×10^3/μL to 4.2×10^3/μL ($p<0.001$). Normal WBC levels range from $5\text{-}12\times10^3$/μL for BALB/c mice [63]. Obviously, the WBC level in the Taxol®-treated group was lesser than the normal range. The WBC count in the PTX-loaded PCL-(SeSe-PEG-FA)$_2$ and PTX-loaded PCL-(SeSe-mPEG)$_2$ groups did not decrease significantly. The mean WBC count of the PTX-loaded PCL-(SeSe-PEG-FA)$_2$ and PTX-loaded PCL-(SeSe-mPEG)$_2$ treated group was 8.1×10^3/μL, which was within the normal range.

The results in Supplementary Figure S3B do not show a significantly abnormal increase in liver function tests (SGOT and SGPT) in groups treated by the micelles. However, the PTX-treated groups had a significant increase in SGOT and SGPT levels, which indicated a decrease in liver function.

3.11. CT and ultrasound images

CT images obtained from the groups treated with PTX and saline showed multiple well-defined sublumbar lymph node invasions with heterogeneous postcontrast enhancement. The PTX-loaded PCL-(SeSe-mPEG)$_2$ and PTX-loaded PCL-(SeSe-PEG-FA)$_2$ groups did not show any significant metastatic lesions nor any lymph node invasion. The main lesions in the saline and Taxol®-treated groups (Fig. S4A) were subjectively larger and more heterogeneous in Hounsfield unit texture compared to the micelle-treated groups (Fig. S4C, D), which contained hypoattenuated lesions.

Figure S4E, F show ultrasound (US) images for the groups treated with saline and Taxol®; multiple, well-defined homogenous, round-to-oval hypo-echo nodules up to 1 cm in length at the level of the subcutaneous lymph nodes were observed. By contrast, US images (Fig. S4G, H) for the PTX-loaded PCL-(SeSe-mPEG)$_2$- and PTX-loaded PCL-(SeSe-PEG-FA)$_2$-treated groups

showed no definite signs that were compatible with any mass lesion in the retroperitoneal and peritoneal regions. Additionally, the subcutaneously induced masses were subjectively smaller and more ill-defined compared to the saline and PTX-treated groups that had heterogeneous hypo- to anechoic echotextures.

4. Conclusion

In this study, a redox-sensitive shell-sheddable micelle based on a PCL-(SeSe-PEG-FA)$_2$ triblock copolymer containing redox-sensitive linkages was successfully synthesized and characterized. The diselenide bonds, as redox-sensitive linkages, located between hydrophilic and hydrophobic segments resulted in the development of the shell-sheddable micelle. The micelles could incorporate a hydrophobic anticancer drug (PTX) into their hydrophobic core. The loaded drug was released by shedding of shell under redox conditions as opposed to drug diffusion. The micelles showed a higher cell internalization rate *through* FR-mediated endocytosis. The diselenide-containing micelles were found to have a better killing effect on 4T1 cells when tested *in vitro* compared to naked drug or insensitive micelles. The PTX-loaded micelles also showed a better antitumor effect and an inhibited tumor growth rate compared to micelles lacking diselenide, in female BALB/c 4T1 tumor-bearing mice. Despite the preliminary stage at which this system is currently in, considering advances made for Genexol and NK-105 reaching clinical testing [64-65], the results depicted the potential of diselenide-containing smart micelles as delivery vehicles for a wide variety of diseases that have abnormal reductive or oxidative environments. We appreciate that costs for clinical studies will be added to the cost of this product; it is, however, estimated that this type of formulation would cost approximately 182$ for 30 mg/vial versus Genexol-PM (30 mg/vial) and PTX (30 mg/vial) costing 167.78 $ [66] and 163.4 $, respectively. The incremental cost effectiveness ratio of this smart carrier versus PTX is approximately 2,000 $ per year, which is above the per capita GDP in our country but in an acceptable range in Europe. Moreover, for the regulatory demands, because the block copolymers used in our study already have an FDA approval, our

only challenge would be obtaining approval for the smart bond. There are many details to be discussed and looked into, which requires further studies and tests.

Acknowledgments

This work was supported by grants from Royan Institute, the Iran National Science Foundation (INSF), and Iran Science Elites Federation to H. B. and F. B. We also thank Thomas Fox at the Department of Chemistry of the University of Zurich for kindly assisting us with the NMR tests.

Competing financial interests

The authors declare no competing financial interests.

Reference

[1] Kataoka K, Harada A, Yu. N, Kataoka K., Harada A, Nagasaki Yu, Block copolymer micelles for drug delivery: design, characterization and biological significance, Adv. Drug Deliv. Rev. 47 (2001) 113-31.

[2] Shin DH, Tam YT, Kwon GS, Polymeric micelle nanocarriers in cancer research, Front. Chem. Sci. Eng. 10 (2016) 348–59.

[3] Min KH, Lee HJ, Kim K, Kwon IC, Jeong SY, Lee SC, The tumor accumulation and therapeutic efficacy of doxorubicin carried in calcium phosphate-reinforced polymer nanoparticles, Biomaterials 33 (2012) 5788–97.

[4] Prabaharan M, Grailer JJ, Pilla S, Steeber DA, Gong S, Amphiphilic multi-arm-block copolymer conjugated with doxorubicin *via* pH-sensitive hydrazone bond for tumor-targeted drug delivery, Biomaterials 30 (2009) 5757–66.

[5] Otsuka H, Nagasaki Y, Kataoka K, PEGylated nanoparticles for biological and pharmaceutical applications, Adv. Drug Deliv. Rev. 55 (2003) 403–19.

[6] Suk JS, Xu Q, Kim N, Hanes J, Ensign LM, PEGylation as a strategy for improving nanoparticle-based drug and gene delivery, Adv. Drug Deliv. Rev. 99 (2016) 28–51.

[7] Cabral H, Kataoka K, Progress of drug-loaded polymeric micelles into clinical studies, J. Control. Release 190 (2014) 465–76.

[8] Tyrrell ZL, Shen Y, Radosz M, Fabrication of micellar nanoparticles for drug delivery through the self-assembly of block copolymers, Prog. Polym. Sci. 35 (2010) 1128–43.

[9] Abandansari HS, Aghaghafari E, Nabid MR, Niknejad H, Preparation of injectable and thermoresponsive hydrogel based on penta-block copolymer with improved sol stability and mechanical properties, Polymer 54 (2013) 1329-40.

[10] Valera-Moreira A, Shi Y, Fens H.M, Lammers T, Hennink W, Schiffelers Raymon M. , Clinical application of polymeric micelles for the treatment of cancer, Royal Society of Chemistry 1 (2017) 1485-1501.

[11] Marin E, Briceno MI,Caballero C, Critical evaluation of biodegradable polymers used in nanodrugs, Int. J. Nanomedicine. 8 (2013) 3071-91.

[12] Wilhelm S, Tavares AJ, Dai Q, Ohta S, Audet J, Dvorak HF, Harold F, Warren C.W., Analysis of nanoparticle delivery to tumours, Nat. Rev. Mater. 1 (2016) 16014.

[13] Mura S, Nicolas J, Couvreur P, Stimuli-responsive nanocarriers for drug delivery, Nat. Mater. 12 (2013) 991–1003.

[14] Xu CF, Zhang HB, Sun CY, Liu Y, Shen S, Yang XZ, Zhu YH,Wang J, Tumor acidity-sensitive linkage-bridged block copolymer for therapeutic siRNA delivery, Biomaterials 88 (2016) 48–59.

[15] Huang F, Wang J, Qu A, Shen L, Liu J, Liu J, Zhang Z, An Y, Shi L, Maintenance of amyloid b peptide homeostasis by artificial chaperones based on mixed-shell polymeric micelles, Angew. Chemie - Int. Ed. 53 (2014) 8985–90.

[16] Sun H, Guo B, Cheng R, Meng F, Liu H, Zhong Z, Biomaterials biodegradable micelles with sheddable poly (ethylene glycol) shells for triggered intracellular release of doxorubicin, Biomaterials 30 (2009) 6358–66.

[17] Ping Liu, Haijun Zhang, Xue Wu, Liting Guo, Fei Wang, Guohua Xia, Baoan Chen, HaiXiang Yin, Yonglu Wang, Xueming Li, Tf-PEG-PLL-PLGA nanoparticles enhanced chemosensitivity for hypoxia-responsive tumor cells, Onco. Targets. Ther. 9 (2016) 5049-59

[18] Yu H, Chen J, Liu S, Lu Q, He J, Zhou Z,Hu Y, Enzyme sensitive, surface engineered nanoparticles for enhanced delivery of camptothecin, J. Control. Release 216 (2015) 111–20.

[19] Moon SY, Choi YS, Cho J.K, Yu M, Lee E, Huh KM,Lee D, Kim J, Kang han Chang, Intracellular thiol-responsive nanosized drug carriers self-assembled by poly(ethylene glycol)-b-poly(ε-caprolactone)-b-poly(ethylene glycol) having multiple bioreducible disulfide linkages in hydrophobic blocks, RSC Adv.6 (2016) 15558–76.

[20] Abandansari HS, Abuali M, Nabid MR, Niknejad H, Enhance chemotherapy efficacy and minimize anticancer drug side effects by using reversibly pH- and redox-responsive cross-linked unimolecular micelles, Polymer 116 (2017) 16-26.

[21] Hanmei Li, Hao Jiang, Mnegnan Zhao, Yao Fu, Xun Sun, Intracellular redox potential-responsive micelles based on polyethylenimine-cystamine-poly(ε-caprolactone) block copolymer for enhanced miR-34a delivery, Polymer Chemistry 6 (2015) 1952-1960.

[22] Ma N, Li Y, Xu H, Wang Z, Zhang X, Dual redox responsive assemblies formed from diselenide block copolymers, J. Am. Chem. Soc. 132 (2010) 442–3.

[23] Xu H, Cao WEI, Zhang XI, Selenium-containing polymers : promising biomaterials for controlled release, Accunts of Chemical Research 46 (2013) 1647-5.

[24] Ma N, Li Y, Ren H, Xu H, Li Z, Zhang X, Selenium-containing block copolymers and their oxidation-responsive aggregates, Polym. Chem. 1 (2010) 1609-1614.

[25] Kryukov G V, Castellano S, Novoselov SV, Lobanov AV, Zehtab O, Guigo R, Gladyshev VN, Characterization of Mammalian Selenoproteomes, Science 300 (2003) 1439– 1443.

[26] El-Bayoumy K, Chae Y.H, Upadhyaya P, Meschter C, Cohen LA, Reddy BS, Inhibition of 7,12-dimethylbenz(a)anthracene-induced tumors and DNA adduct formation in the mammary glands of female Sprague-Dawley rats by the synthetic organoselenium compound, 1,4-phenylenebis(methylene)selenocyanate, Cancer Res. 52 (1992) 2402–7.

[27] Ip C, Thompson HJ, Ganther HE, Selenium modulation of cell proliferation and cell cycle biomarkers in normal and premalignant cells of the rat mammary gland, Cancer Epidemiol. Biomarkers Prev. 9 (2000) 49–54.

[28] Raich PC, Lu J, Thompson HJ, Combs Jr. GF, Selenium in cancer prevention: clinical issues and implications, Cancer Invest 19 (2001) 540–53.

[29] Yu SY, Ao P, Wang LM, Huang SL, Chen HC, Lu XP, Liu QY, Biochemical and cellular aspects of the anticancer activity of selenium, Biol Trace Elem Res 15 (1988) 243–55.

[30] Sun T, Jin Y, Qi R, Peng S, Fan B, Oxidation responsive mono-cleavable amphiphilic diblock polymer micelles labeled with a single diselenide, Polym. Chem. 4 (2013) 4017.

[31] Chao Wei, Yan Zhang, Zhongchen Song, Yiru Xia, Heng Xu, Meidong Lang, Enhanced bioreduction-responsive biodegradable diselenide-containing poly(ester urethane) nanocarriers, Biomaterials Science 5 (2017) 669-677.

[32] Grant L. Zwicke, G. Ali Mansoori, Constance J. Jeffery, Utilizing the folate receptor for active targeting of cancer nanotherapeutics, Nano Reviews 20 (2012) 10095–109.

[33] J.A Ledermann, S. Canevari, T. Thigpen, Targeting the folate receptor: diagnostic and therapeutic approaches to personlized cancer treatments, Annals of Oncology 26(2015) 2034-2043

[34] Rafique J, Saba S, Canto RFS, Frizon TEA, Hassan W, Waczuk EP, Jan M, Back DF, Da Rocha JB, Braga AL, Synthesis and biological evaluation of 2-picolylamide-based diselenides with non-bonded interactions, Molecules 20 (2015) 10095–109.

[35] Mohapatra S, Mallick SK, Maiti TK, Ghosh SK, Pramanik P. Synthesis of highly stable folic acid conjugated magnetite nanoparticles for targeting cancer cells, Nanotechnology 18 (2007) 385102.

[36] Abouelmagd SA, Sun B, Chang AC, Ku YJ, Yeo Y, Release kinetics study of poorly water-soluble drugs from nanoparticles: Are we doing it right?, Mol. Pharm. 12 (2015) 997–1003.

[37]Mao F, Paclitaxel, USP29-NF24 30 (1010) 1279. http://www.pharmacopeia.cn/v29240/usp29nf24s0_m60190.html

[38] Biswas S, Dodwadkar NS, Deshpande PP, Torchilin VP, Liposomes loaded with paclitaxel and modified with novel triphenylphosphonium-PEG-PE conjugate possess low toxicity, target mitochondria and demonstrate enhanced antitumor effects *in vitro* and *in vivo*, J. Control. Release 159 (2012) 393–402.

[39] Rivolta I, Panariti A, Lettiero B, Sesana S, Gasco P, Gasco MR, Masserini M, Miseroochi G, Cellular uptake of coumarin-6 as a model drug loaded, J. Physiol Pharmacol. 62 (2011) 45–53.

[40] Li R, Li X, Xie L, Ding D, Hu Y, Qian X, Yu L, Ding Y, Jiang X, Liu B, Preparation and evaluation of PEG–PCL nanoparticles for local tetradrine delivery, Int. J. Pharma. 379 (2009) 158–66.

[41] Sun Y, Zou W, Bian S, Huang Y, Tan Y, Liang J, Fan Y, Zhang Xingdong, Bioreducible PAA- g -PEG graft micelles with high doxorubicin loading for targeted antitumor effect against mouse breast carcinoma, Biomaterials 34 (2013) 6818–28.

[42] Xue J, Chi Y, Chen Y, Huang S, Ye X, Niu J, Wang W, Pfeffer LM, Shao ZM, Wu ZH, Wu J, MiRNA-621 sensitizes breast cancer to chemotherapy by suppressing FBXO11 and enhancing p53 activity, Oncogene 35 (2016) 448–58.

[43] Green RM, Flamm S, AGA technical review on the evaluation of liver chemistry tests, Gastroenterology 123 (2002) 1367–84.

[44] Wei C, Zhang Y, Xu H, Xu Y, Lang M, Well-defined labile diselenide-centered poly(e-caprolactone)-based micelles for activated intracellular drug release, J. Mater. Chem. B. 4 (2016)

5059-67.

[45] Zhao C, Winnik MA, Croucher MD, Fluorescence probe techniques used to study micelle formation in water-soluble block copolymers, J. Am. Chem. Soc. 6 (1990) 514–6.

[46] Basu Ray G, Chakraborty I, Moulik SP, Pyrene absorption can be a convenient method for probing critical micellar concentration (cmc) and indexing micellar polarity, J. Colloid Interface Sci. 294 (2006) 248–54.

[47] Ramasamy T, Ruttala HB, Kanu BG, Poudel BK, Choi H, Yong CS, Kim oh Jong, Smart chemistry-based nanosized drug delivery systems for systemic applications: A comprehensive review, J. Control Release 258 (2017) 226-53.

[48] Szatrowski TP, Nathan CF, Production of large amounts of hydrogen peroxide by human tumor cells, Cancer Res. 51 (1991) 794–9.

[49] Eun Kyoung Park, So Yeon kim, Sang Bong Lee, Young Moo Lee, Folate-conjugated methoxy poly(ethylene glycol)/poly(ε-caprolactone) amphiphilic block copolymeric micelles for tumor-targeted drug delivery, Journal of Control Release 109 (2005) 158-168

[50] Wei Xiong, Lixia Peng, Hongbo Chen, Qin Lin, Surface modification of MPEG-*b*-PCL-based nanoparticles via oxidative self-polymerization of dopamine for malignant melanoma therapy, 10 (2015) 2985-2996.

[51] Gong J. Huo M, Zhou J, Zhang Y, Peng X, Yu D, Zhang H, Li J, Synthesis, characterization, drug-loading capacity and safety of novel octyl modified serum albumin micelles, International Journal of Pharmaceutics 376 (2009) 161-168,

[52] Zachary L. Tyrrell, Youqing Shen, Maciej Radsoz, Near-Critical Fluid Micellization for High and Efficient Drug Loading: Encapsulation of Paclitaxel into PEG-*b*-PCL Micelles, 115 (2011) 11951-11956.

[53] Evan Krystofiak, Vyara Matson, Douglas Steeber, Julie Oliver, Elimination of tumor cells using folate receptor targeting by anti-body-conjugated, gold coated magnetite nanoparticles in a murine breast cancer model, Journal of Nanomaterials 4 (2012) 1155-65.

[54] Park EK, Kim SY, Lee SB, Lee YM, Folate-conjugated methoxy poly (ethylene glycol)/ poly (q -caprolactone) amphiphilic block copolymeric micelles for tumor-targeted drug delivery, Biomaterials 109 (2005) 158–68.

[55] Zhang Y, Zhang H, Wang X, Wang J, Zhang X, Zhang Q, The eradication of breast cancer and cancer stem cells using octreotide modi fi ed paclitaxel active targeting micelles and salinomycin passive targeting micelles, Biomaterials 33 (2011) 679-91.

[56] Yokoyama M, Drug targeting with nano-sized carrier systems, J Artif Organs, 8 (2005), 77-

84.

[57] Bae YH, Park K, Targeted drug delivery to tumors: Myths, reality and possibility, J. Control Release 153 (2011) 198–205.

[58] Rezazadeh M, Emami J, Lavasanifar A, In vivo pharmacokinetics, bio distribution and anti-tumor effect of paclitaxel-loaded targeted chitosan-based polymeric micelle, Drug delivery 23 (2016) 1707-17.

[59] Yerlikaya A, Erin N, Differential sensitivity of breast cancer and melanoma cells to proteasome inhibitor Velcade, Int J Mol Med 22 (2008) 817-23.

[60] Meri Kuo, Al-Jamal K, Investigating the effect of tumor vascularization on magnetic targeting in vivo using retrospective design of experiment, Biomaterials 106 (2016) 276-85.

[61] Gilbert S. A, Conceptual History of Modern Embryology, JHU Press, Baltimore, USA, 1991.

[62] Yi X, Lian X, Dong J, Wan Z, Xia C, Song X, Fu Y, Gong T, Zhang Z, Co-delivery of pirarubicin and paclitaxel by human serum albumin nanoparticles to enhance antitumor effect and reduce systemic toxicity in breast cancers, Mol. Pharm. 12 (2015) 4085-98.

[63] BALB / c Nude Mouse Hematology Mouse Biochemistry. https://www.criver.com/sites/default/files/resources/ , 2012

[64] Michael E. Werner,Natalie D. Cummings, BS,Manish Sethi, Edina C. Wang, Rohit Sukumar, Dominic T. Moore, Andrew Z. Wang, Preclinical Evaluation of Genexol-PM, a Nanoparticle Formulation of Paclitaxel, as a Novel Radiosensitizer for the Treatment of Non-Small Cell Lung Cancer, Int J Radiat Oncol Biol Phys. 86 (2014) 463-468.

[65] Hamaguchi T, Matsumura Y, Suzuki M, Shimizu K, Goda R, Nakamura I, Nakatomi I, Yokoyama M, Kataoka K, Kakizoe T, NK105, a paclitaxel-incorporating micellar nanoparticle formulation, can extend *in vivo* antitumour activity and reduce the neurotoxicity of paclitaxel, Br J Cancer 92 (2005) 1240-1246.

[66] Kim J, Shin S, Cost-effectiveness of Genexol-PM for treating Metastatic Breast Cancer, Journal of Breast Cancer 13 (2010) 104-110.

Scheme legend

Scheme 1. Schematic illustration of micelle formation and mechanism of drug release from responsive micelles in a redox environment of cancer cells.

Figure legends

Fig. 1. Synthesis of diselenide (A) PCL-bis(SeSe-PEG)$_2$ copolymers (B), and PCL bis(SeSe-PEG-FA)$_2$ (C).

Fig. 2. ^{77}Se-NMR (A) and ^{1}H,^{77}Se-HMBC (B)spectra of diselenide.

Fig. 3. ^{1}H-NMR spectra of 10-bromodecanoic acid (A), diselenide (B), (PCL-SeSe-COOH)$_2$ (C), mPEG-OTS (D), m-PEG amine (E), and mPEG-(PCL-SeSe)$_2$ (F).

Fig. 4. Determination of the critical micelle concentration (CMC): Excitation spectra of pyrene in an aqueous solution of micelles at various concentrations ($\lambda_{emission}$: 372 nm) (I) and intensity ratio (I_{372}/I_{384}) as a function of micelle concentration (II) (A). Particle size and size distribution of micelles: Dynamic light scattering (DLS) of PCL-(SeSe-mPEG)$_2$ and PCL-(mPEG)$_2$ under different conditions (2 mM GSH, 0.1% wt. H_2O_2 and DPBS). Three batches for each micelle group with triplicates of each batch (3*3=9 set of tests for each group) were tested with DLS (B). Representative transmission electron microscopy (TEM) of micelles PCL-(SeSe-mPEG)$_2$. Scale bar: 200 nm (C).

Fig. 5. Cell survival and cumulative release of micelles. Time-dependent thiol-triggered and oxidative drug release of drug-loaded micelles in PBS, 0.1% wt. H_2O_2 and 2 mM GSH buffer at 37°C. Comparisons were made among diselenide containing micelles and PCL-(mPEG)+PTX (A). Cytotoxicity for 4T1 cells treated after 24 h with PCL-(mPEG)$_2$, PCL-(SeSe-PEG-FA)$_2$, PCL-(SeSe-mPEG)$_2$, and antitumor activity of carriers versus the concentration of PTX for 4T1 cells treated with Taxol®, PCL-(mPEG)$_2$+PTX, PCL-(SeSe-PEG-FA)$_2$+PTX, and PCL-(SeSe-mPEG)$_2$+PTX. PTX concentrations that caused inhibition of 50% cell viability (IC50 values) were determined by sigmoidal fitting as 55 nM for Taxol®, 1 nM for PCL-(SeSe-PEG-FA)$_2$+PTX, and 10 nM for PCL-(SeSe-mPEG)$_2$+PTX. ***: PCL-(mPEG) +PTX vs. PTX, PCL-(mPEG)+PTX vs. PCL-(SeSe-PEG-Folate)$_2$+PTX, PCL-(mPEG)$_2$+PTX vs. PCL-(SeSe-mPEG)$_2$+PTX; **: PCL-(mPEG)$_2$+PTX vs. PCL-(SeSe-mPEG)$_2$+PTX; ***: PCL-(mPEG)$_2$+PTX vs. PCL-(SeSe-mPEG)$_2$+PTX (B). Each experiment was repeated thrice, and this is a representative of all. The IC50 value was calculated and analyzed by the Newman−Keuls test following one-way ANOVA. The data were expressed as mean ± SEM. Error bars are based on

three parallel samples. Plain micelles (without PTX) were nontoxic. *p<0.05, **p<0.01, ***p < 0.001 (n=3).

Fig. 6. Cellular uptake and distribution of drug-loaded micelles in 4T1 cells. Cellular uptake measured 4 h post-treatment by flow cytometry. The cells were treated with coumarin-6–loaded PCL-(SeSe-mPEG)$_2$ and PCL-(SeSe-PEG-FA)$_2$ as well as coumarin-6. Folate-conjugated micelles showed better cellular uptake (I). Comparison of qualitative cellular uptake efficiency between coumarin-6–loaded PCL-(SeSe-mPEG)$_2$ and coumarin-6–loaded PCL-(SeSe-PEG-FA)$_2$. Data are represented as mean ± SD (n=3) (II) (A). Cellular distribution of 4T1 cells 4 h post-treatment with PCL-(SeSe-mPEG)$_2$+coumarin-6 and PCL-(SeSe-PEG-FA)$_2$+coumarin-6 using confocal laser scanning microscopy (CLSM). The cell nucleus was stained blue (DAPI), and the green stains were coumarin-6 (scale bar: 50 µm). We observed a higher cell uptake in the folate-conjugated micelles (B). Each experiment was repeated thrice. The cellular uptake value was calculated and analyzed by the Newman−Keuls test following one-way ANOVA. The data were expressed as mean ± standard deviation. ***: p<0.001 (n=9).

Fig. 7. Tumor growth inhibition and body weight changes in BALB/c 4T1 tumor-bearing mice. Mice received intraperitoneal (i.p.) injections with a 15 mg/kg PTX equivalent dose: PTX-loaded PCL-(SeSe-mPEG)$_2$ and PCL-(SeSe-PEG-FA)$_2$, control (saline), and Taxol®. The mice received six i.p. injections on days 0, 4, 8, 12, 16, and 20. We observed better therapeutic effects in diselenide-containing micelles than in the other treatment groups (A). Body weight changes in similar groups. There was no significant weight loss observed in mice treated with diselenide micelles compared to the other treatment groups. ***p<0.001 (*** and ****: micelles vs. the other two groups) (B). The data were analyzed by the Newman−Keuls test following one-way ANOVA. Tumor volume and weight values are represented as mean ± SEM. *p<0.05, **p<0.01, ***p < 0.001 (n=6).

Fig. 8. Histological assessments with hematoxylin and eosin (H&E) staining of vital organs from female BALB/c 4T1 tumor-bearing mice treated with intraperitoneal (i.p.) injections of Taxol®, PCL-(SeSe-mPEG)$_2$+PTX, PCL-(SeSe-PEG-FA)$_2$+PTX, and control (saline) (heart, kidneys, liver, spleen, and lungs). These are representative sections from five mice per group. The organs were harvested at day 30 post injection. We observed the following effects: Zenker's necrosis,

mild hyperemia, myocardial atrophy, myofibrillar loss, and cell atrophy (black arrows). Histological analysis was conducted after H&E staining. Scale bar: 200 μm.

Fig. 9. Hematoxylin and eosin (H&E) and Ki-67 staining analysis of tumor sections in female BALB/c 4T1 tumor-bearing mice treated with intraperitoneal (i.p.) injections of Taxol®, PCL-(SeSe-mPEG)$_2$+PTX, and PCL-(SeSe-PEG-FA)$_2$+PTX. The cytoplasm stained light red by eosin, whereas the cell nucleus stained purple with hematoxylin (H&E staining). The green stains indicated Ki-67-positive staining areas and nuclei in the Ki-67 assay, respectively. Images are representative sections from five mice per group. The organs were harvested at day 30. Scale bar: 200 μm (A). Necrosis of the tumor tissue was quantified using H&E images (I). Proliferation of tumor cells was quantified using Ki-67 staining images (II) (*, **, ***: micelle groups compared to the control) (B). Necrosis of the tumor tissue and proliferation index were calculated and analyzed by the Newman−Keuls test following one-way ANOVA. Data were expressed as mean ± standard deviation. *$p<0.05$, **$p<0.01$, *** $p<0.001$. Data are represented as the mean ± SD (n=6).

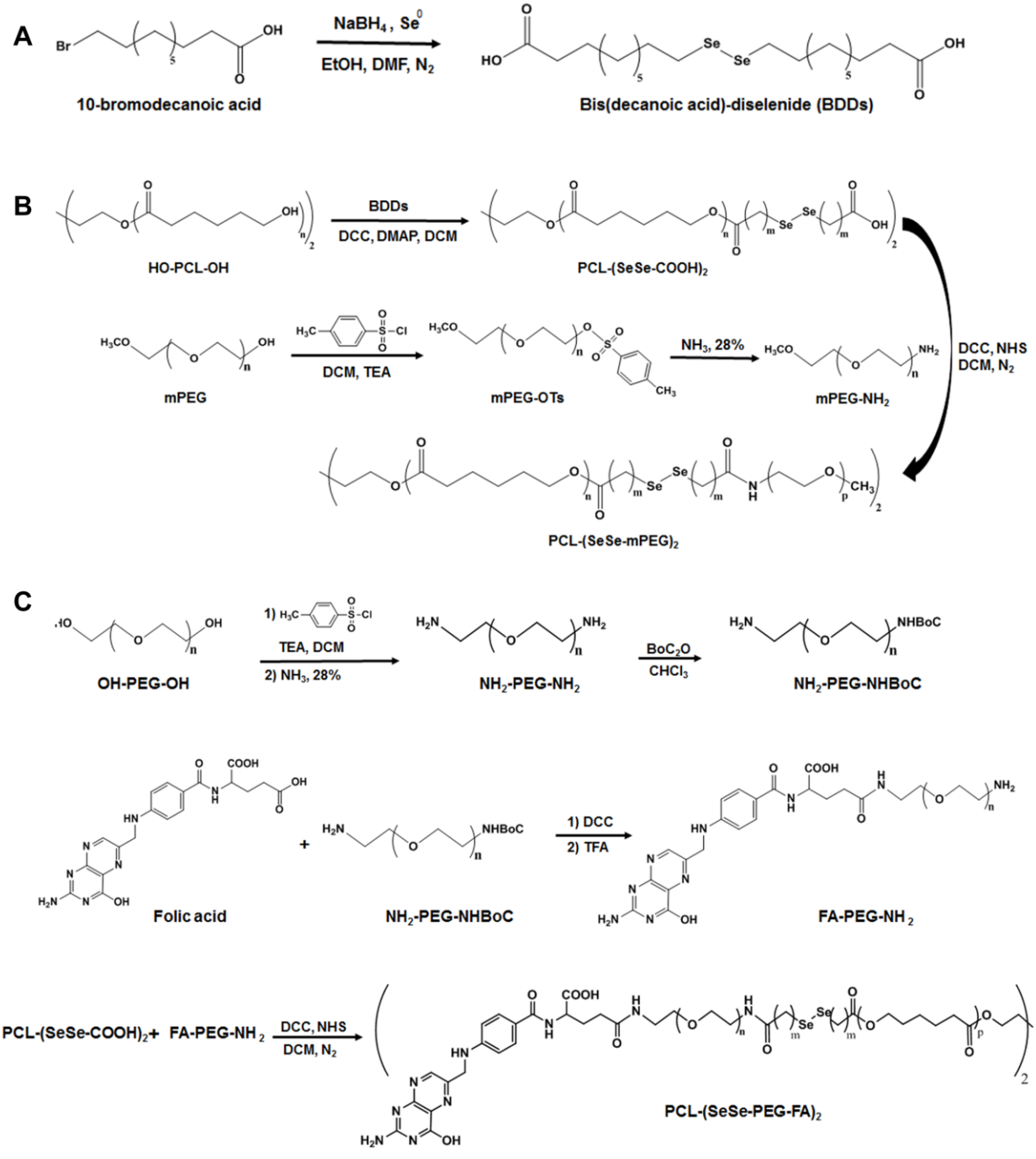
A
NaBH4 , Se0
EtOH, DMF, N2
10-bromodecanoic acid
Bis(decanoic acid)-diselenide (BDDs)
B
BDDs
DCC, DMAP, DCM
HO-PCL-OH
PCL-(SeSe-COOH)2
mPEG
DCM, TEA
mPEG-OTs
NH3, 28%
mPEG-NH2
DCC, NHS
DCM, N2
PCL-(SeSe-mPEG)2
C
OH-PEG-OH
1) TEA, DCM
2) NH3, 28%
NH2-PEG-NH2
BoC2O
CHCl3
NH2-PEG-NHBoC
Folic acid
NH2-PEG-NHBoC
1) DCC
2) TFA
FA-PEG-NH2
PCL-(SeSe-COOH)2+ FA-PEG-NH2
DCC, NHS
DCM, N2
PCL-(SeSe-PEG-FA)2

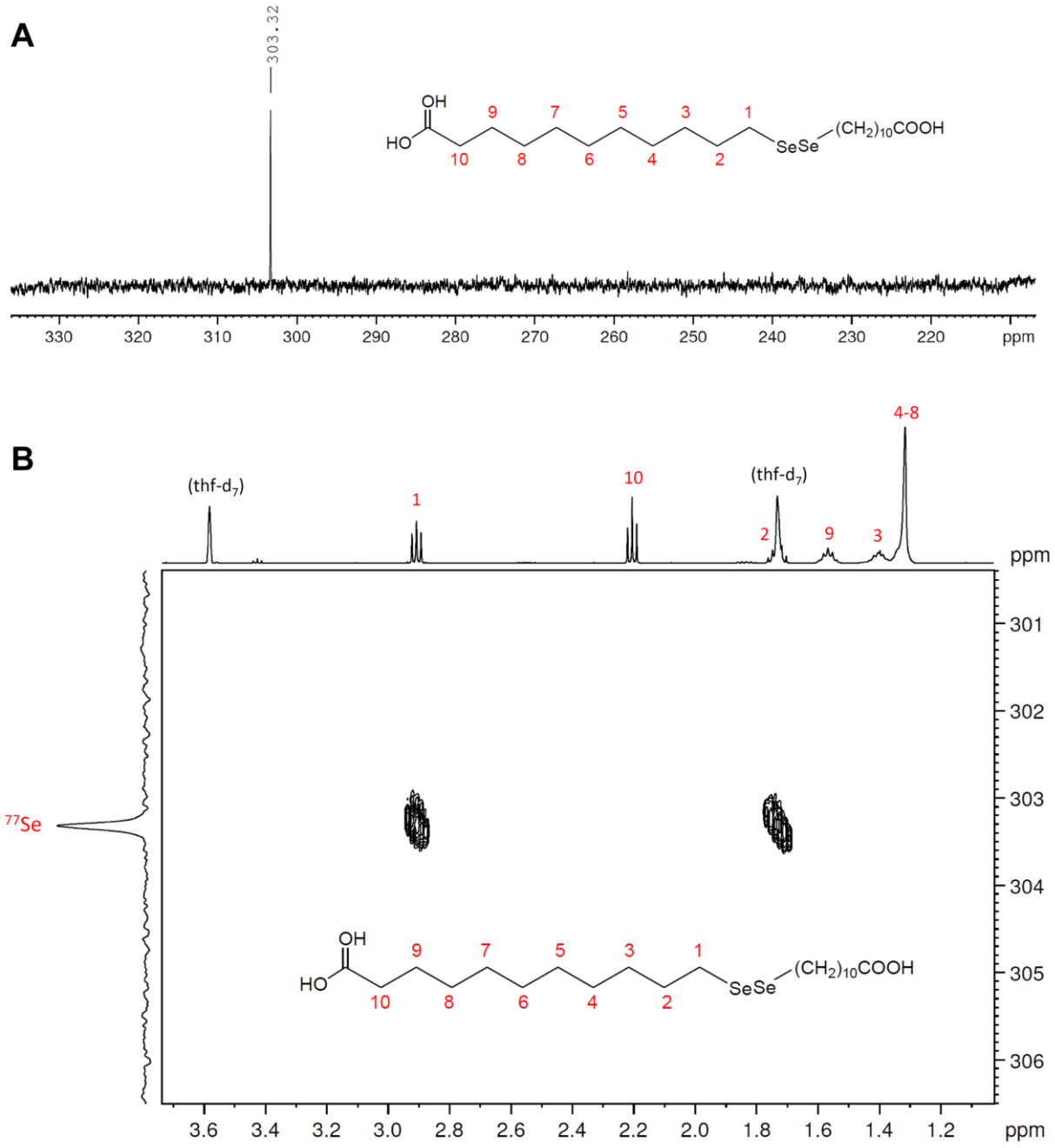
A
303.32
OH
HO
9
7
5
3
1
10
8
6
4
2
SeSe
(CH2)10COOH
330
320
310
300
290
280
270
260
250
240
230
220
ppm
B
(thf-d7)
1
10
(thf-d7)
4-8
2
9
3
ppm
77Se
301
302
303
304
305
306
3.6
3.4
3.2
3.0
2.8
2.6
2.4
2.2
2.0
1.8
1.6
1.4
1.2
ppm

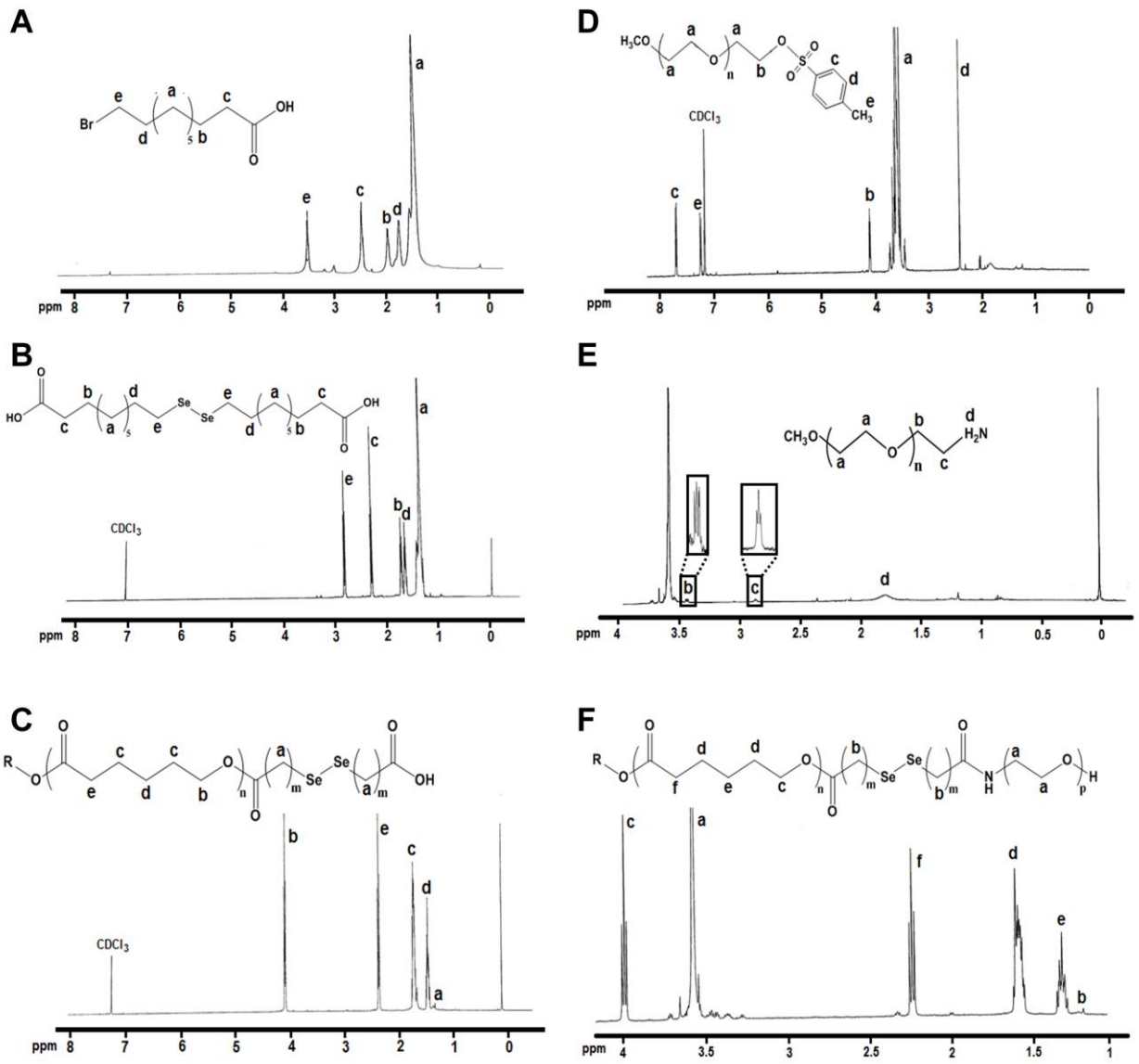
A
B
C
D
E
F
CDCl3
ppm

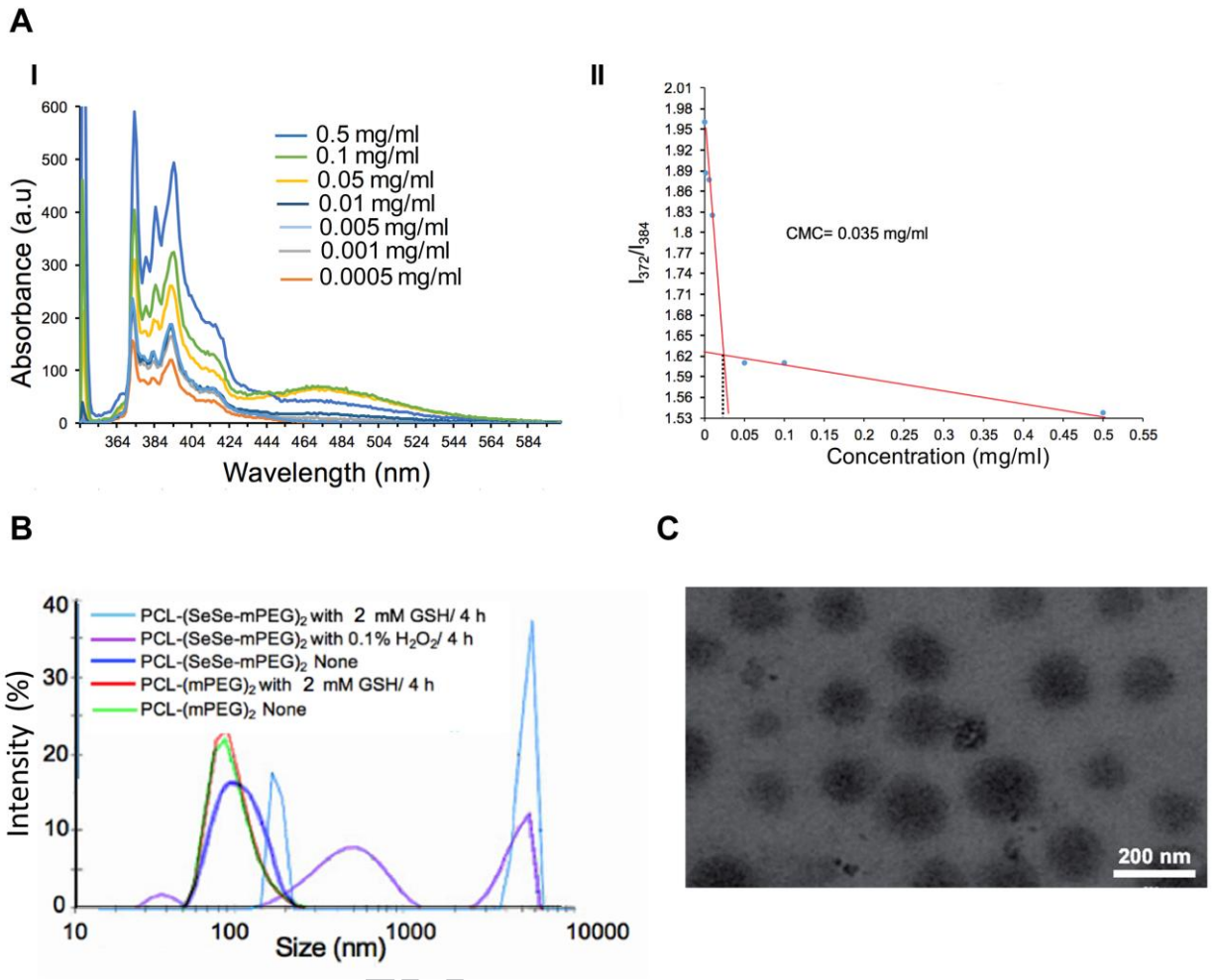
A
I
Absorbance (a.u)
Wavelength (nm)
0.5 mg/ml
0.1 mg/ml
0.05 mg/ml
0.01 mg/ml
0.005 mg/ml
0.001 mg/ml
0.0005 mg/ml
II
I_{372}/I_{384}
CMC= 0.035 mg/ml
Concentration (mg/ml)
B
Intensity (%)
Size (nm)
PCL-(SeSe-mPEG)2 with 2 mM GSH/ 4 h
PCL-(SeSe-mPEG)2 with 0.1% H2O2/ 4 h
PCL-(SeSe-mPEG)2 None
PCL-(mPEG)2 with 2 mM GSH/ 4 h
PCL-(mPEG)2 None
C
200 nm

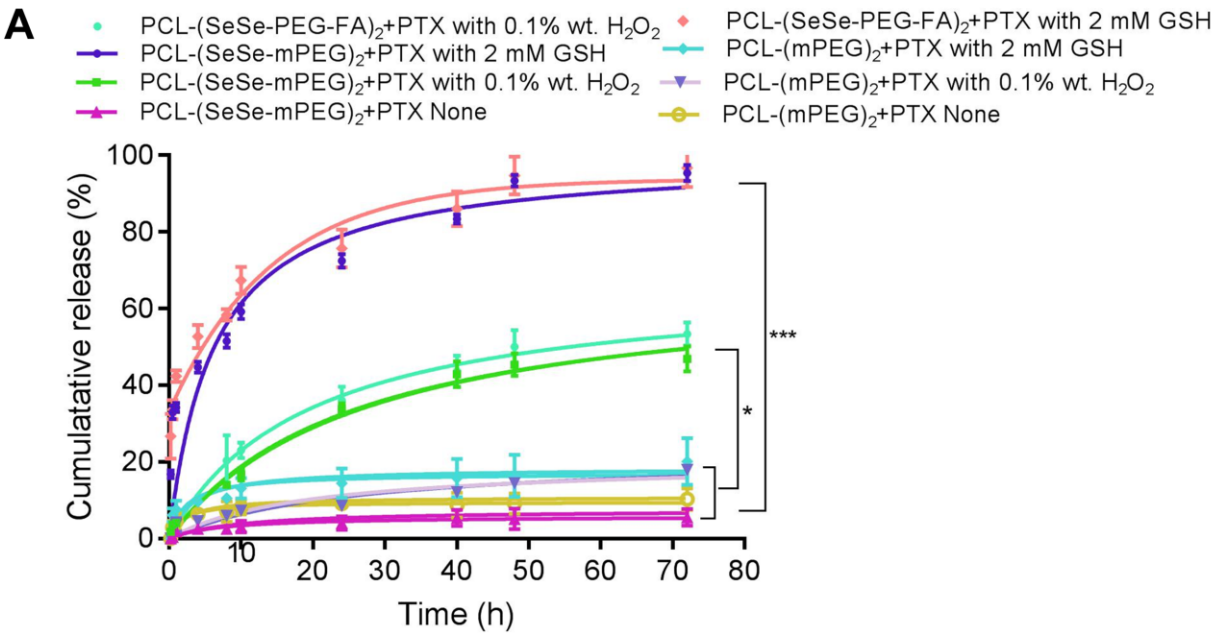
A
PCL-(SeSe-PEG-FA)2+PTX with 0.1% wt. H2O2
PCL-(SeSe-mPEG)2+PTX with 2 mM GSH
PCL-(SeSe-mPEG)2+PTX with 0.1% wt. H2O2
PCL-(SeSe-mPEG)2+PTX None
PCL-(SeSe-PEG-FA)2+PTX with 2 mM GSH
PCL-(mPEG)2+PTX with 2 mM GSH
PCL-(mPEG)2+PTX with 0.1% wt. H2O2
PCL-(mPEG)2+PTX None
Cumulatative release (%)
Time (h)
***
*

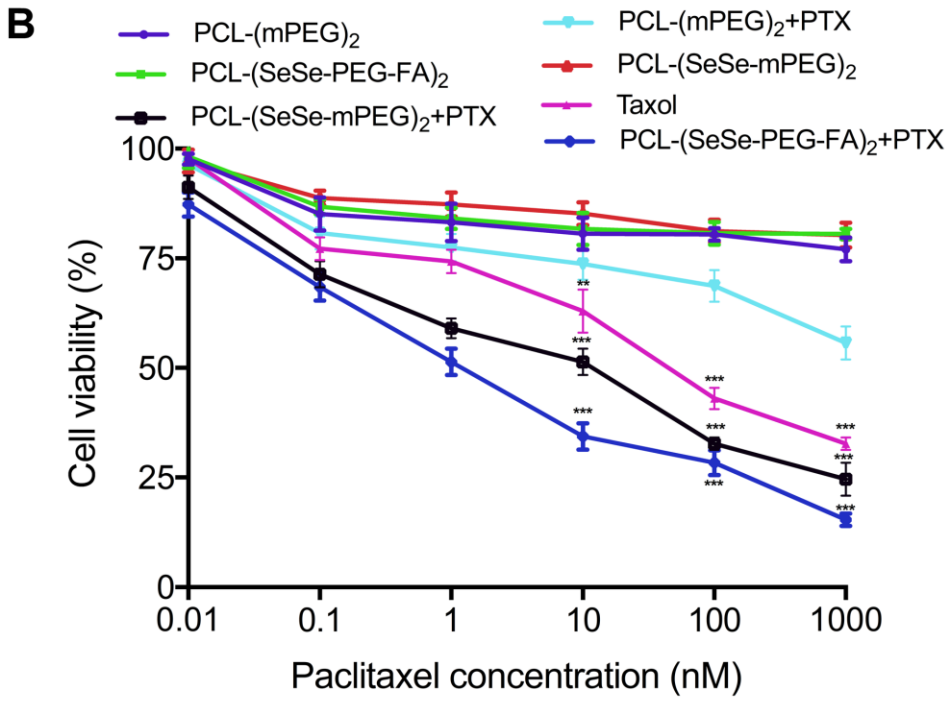
B
PCL-(mPEG)2
PCL-(SeSe-PEG-FA)2
PCL-(SeSe-mPEG)2+PTX
PCL-(mPEG)2+PTX
PCL-(SeSe-mPEG)2
Taxol
PCL-(SeSe-PEG-FA)2+PTX
Cell viability (%)
Paclitaxel concentration (nM)

Fig. 6

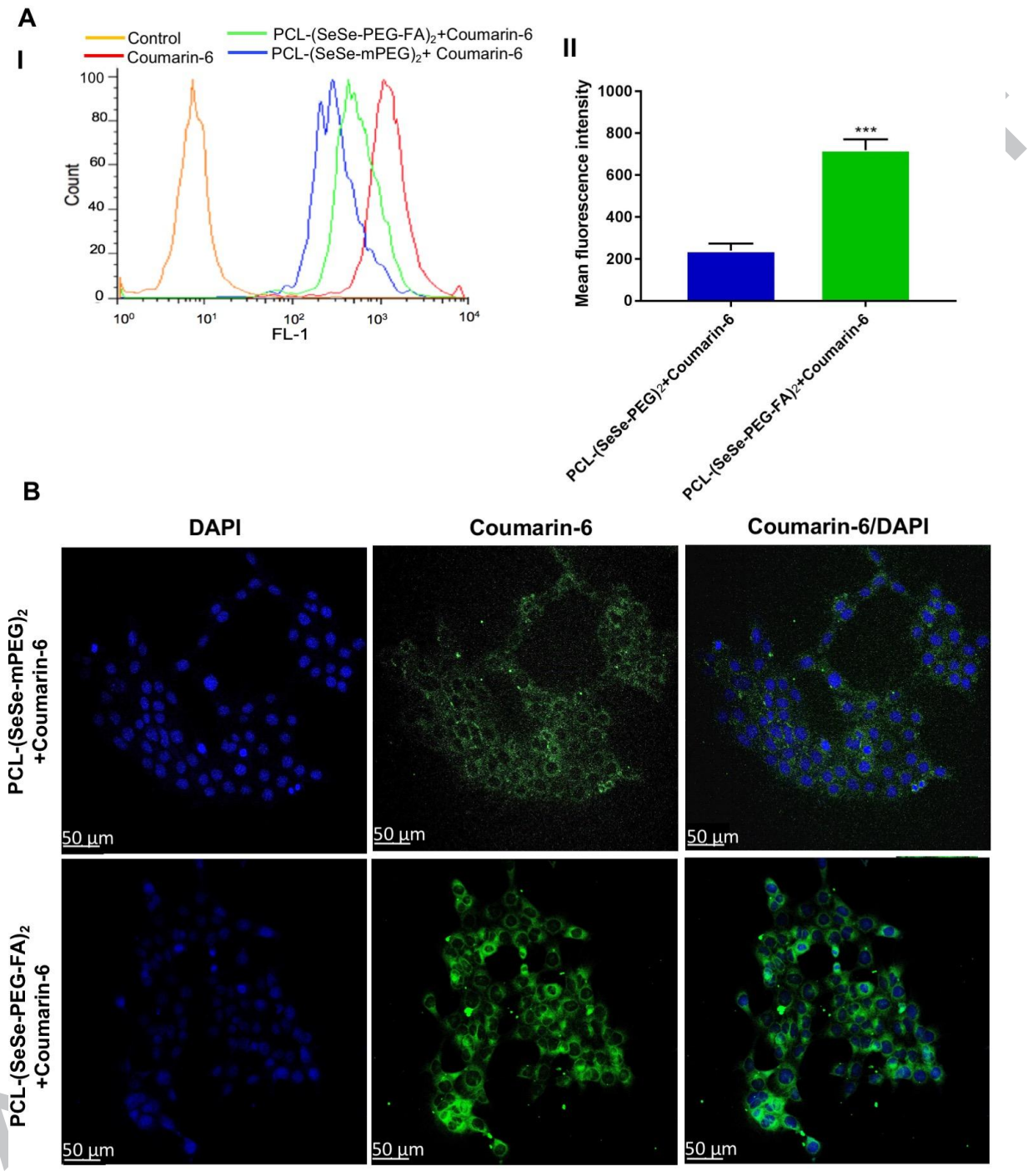
A
I
Control
Coumarin-6
PCL-(SeSe-PEG-FA)2+Coumarin-6
PCL-(SeSe-mPEG)2+ Coumarin-6
Count
FL-1
II
Mean fluorescence intensity
***
PCL-(SeSe-PEG)2+Coumarin-6
PCL-(SeSe-PEG-FA)2+Coumarin-6
B
DAPI
Coumarin-6
Coumarin-6/DAPI
PCL-(SeSe-mPEG)2 +Coumarin-6
PCL-(SeSe-PEG-FA)2 +Coumarin-6
50 µm

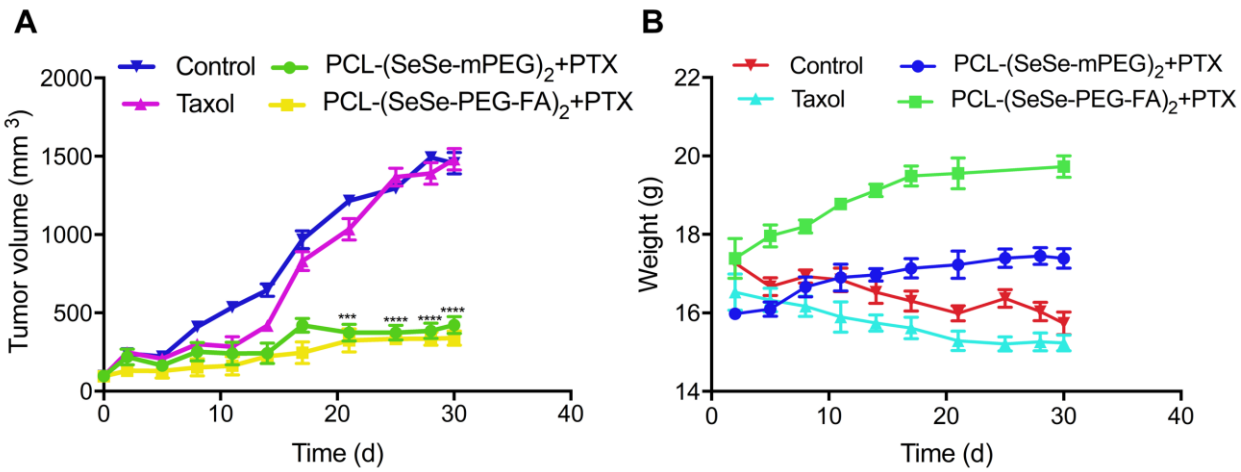

Fig. 8

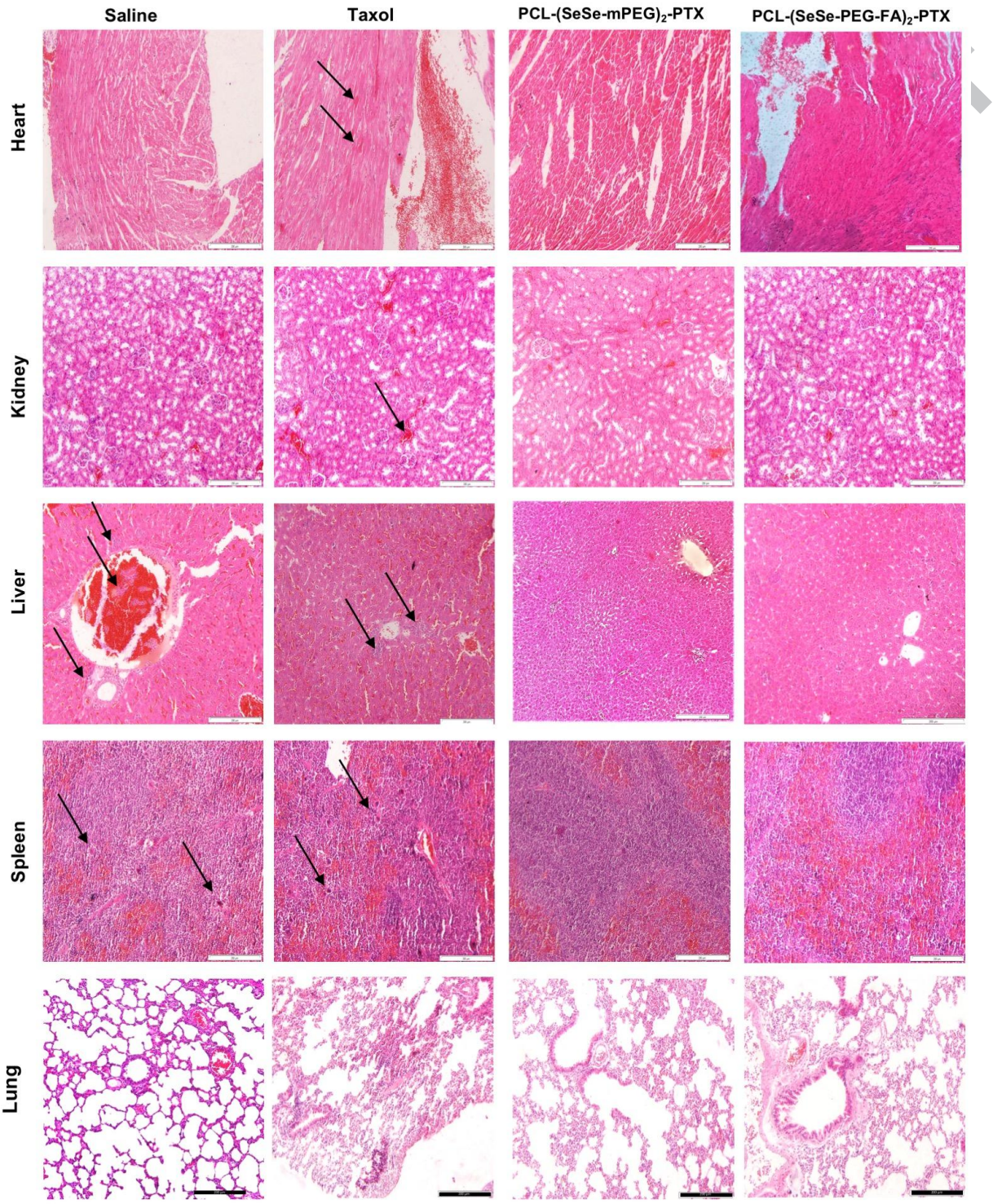
Saline
Taxol
PCL-(SeSe-mPEG)2-PTX
PCL-(SeSe-PEG-FA)2-PTX
Heart
Kidney
Liver
Spleen
Lung

Fig. 9

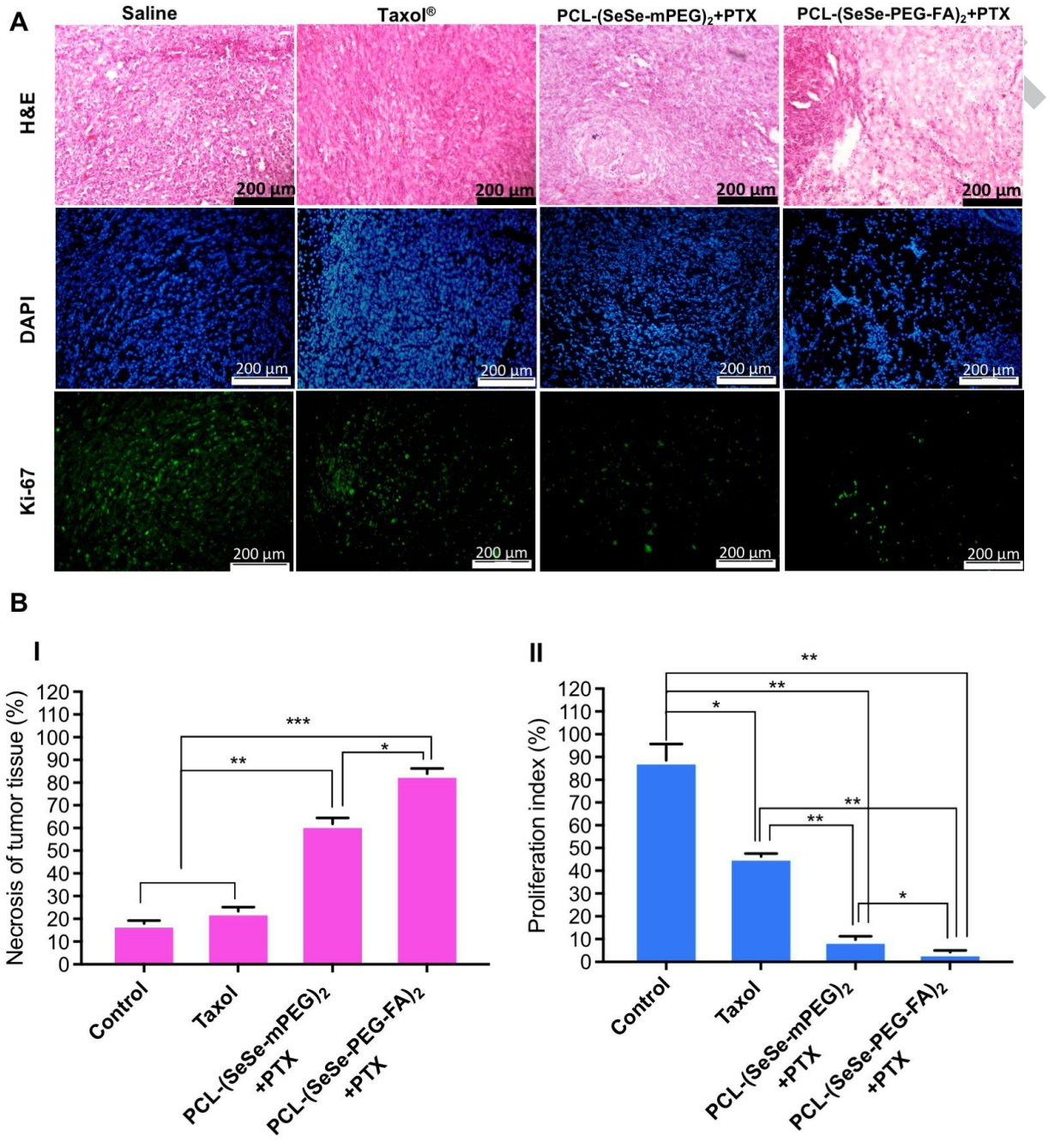
A
Saline
Taxol®
PCL-(SeSe-mPEG)2+PTX
PCL-(SeSe-PEG-FA)2+PTX
H&E
DAPI
Ki-67
200 μm
B
I
Necrosis of tumor tissue (%)
Control
Taxol
PCL-(SeSe-mPEG)2 +PTX
PCL-(SeSe-PEG-FA)2 +PTX
II
Proliferation index (%)

On-demand drug actuation is highly desired. Redox-responsive polymeric DDSs have been shown to be able to respond and release their cargo in a selective manner when encountering a significant change in the potential difference, such as that present between cancerous and healthy tissues. This study offers an added advantage to the field of redox-responsive polymers by reporting a new type of shell-sheddable micelle based on an amphiphilic triblock co-polymer, containing diselenide as a redox-sensitive linkage. The linkage was smartly located at the hydrophilic-hydrophilic bridge in the co-polymer offering complete collapse of the micelle when exposed to the right trigger. The system was able to delay tumor growth and reduce toxicity in a breast cancer tumor model following intraperitoneal injection in mice.